Distributed Beamforming for Wireless Sensor Networks With Improved Graph Connectivity and Energy Efficiency

Keyvan Zarifi, *Member, IEEE*, Ali Ghrayeb, *Senior Member, IEEE*, and Sofiène Affes, *Senior Member, IEEE*

***Abstract*—As the nodes in wireless sensor networks (WSNs) are independent units, an intensive communication among them is required to generate a common signal and synchronize before entering a distributed beamforming (DBF) phase. Therefore, it is crucial to select the participating nodes in DBF such that not only the resulting beampattern meets the beamforming design requirements but also the internode connectivity is retained.**

We consider a DBF technique for WSNs with uniformly distributed nodes and derive an average beampattern expression for a general scenario wherein the participating nodes in DBF are located on a ring with arbitrary inner and outer radii. It is proved that increasing the ring inner radius from zero to a value close to the ring outer radius, the width of the average beampattern mainlobe continuously decreases. Further, it is shown that selecting the nodes from a neighborhood close to a disc perimeter, that is, choosing the nodes from the narrow ring adjacent to the inner side of the disc boundary, facilitates a substantial decrease in the network energy waste and the node isolation probability compared to the case that the nodes are randomly selected from the whole disc. A simple approximate expression for the average beampattern is obtained in the case where the nodes are selected from a narrow ring and is used to derive the sidelobes' null and peak positions as well as a tight lower bound on the average beampattern directivity. The proposed technique is then extended to the case where the nodes are located on multiple concentric rings and the set of rings' radii are derived that guarantee an average beampattern null at a required position while substantially decreasing the sidelobe peak levels compared to the single-ring case. Finally, an average beampattern expression is obtained in the case that the nodes' signals are contaminated by noise to show that most properties of the average beampattern in the noise-free signal case carry over to the noisy signal scenario.

***Index Terms*—Beampattern, distributed beamforming, energy efficiency, network connectivity, wireless sensor network.**

I. Introduction

ONE of the major problems in wireless sensor networks (WSNs) is to establish a reliable communication link between small battery-powered sensor nodes and an access point (AP) that may be located far beyond the nodes' limited transmission range. Adopting the transmit beamforming approach from the centralized array processing literature, distributed beamforming (DBF) for WSNs has recently been proposed to tackle the above problem. In DBF, each node among a set of selected nodes transmits a properly weighted version of (an estimate of) a common signal such that all transmitted signals are coherently combined in the direction of the intended AP. As a result, the nodes aggregate transmission range is substantially increased without requiring to amplify their transmission power. As an effective solution to the problem of long distance communication in WSNs, the DBF approach has received a growing attention [1]–[9].

Assuming that the DBF nodes (the nodes that participate in DBF) are uniformly distributed on a disc, DBF beampattern properties are analyzed in [1] where it is shown that a narrow average beampattern mainlobe entails selecting the DBF nodes from a large cluster in the network. The results of [1] are then extended to two-dimensional Gaussian distributed nodes in [2] and to ad-hoc networks with multiple simultaneous source-destination pairs in [3]. The feasibility of DBF in presence of synchronization errors is investigated and a distributed synchronization technique is proposed in [4]. Assuming a finite-rate feedback on the channel state information from the AP, a DBF technique is proposed in [5] that minimizes the total average transmit power subject to average rate and bit-error rate (BER) requirements. Considering a two-step amplify-and-forward protocol, [6] and [7] propose several DBF techniques subject to total and per-node power constraints as well as signal-to-noise ratio (SNR) requirements. A robust DBF technique against channel estimation errors is introduced in [8] and an overview on current challenges and progresses of the DBF approach is presented in [9].

A common denominator in most DBF approaches including [1]–[9] is the implicit assumption that the DBF network is interconnected, for otherwise, implementing a DBF technique is practically impossible in most cases. Note that when implementing a DBF technique in a real world scenario, one typically has to deal with two main challenges: First, as the nodes in WSNs are independent sensing units, their common signal may need to be generated through a rumor spreading or a consensus process [10]–[12] among the nodes. Second, as the nodes do not have a common time reference, they should synchronize with one another [1], [4], [13] to be able to coordinate the transmission of their common signal. These prerequisite steps necessitate intensive internode communications prior to the actual DBF procedure. Therefore, it is crucial that the DBF nodes form

Manuscript received December 03, 2008; accepted October 19, 2009. First published November 20, 2009; current version published February 10, 2010. This work was supported in part by the NSERC under Grant N00858, in part by a Canada research chair in high-speed wireless communications, the strategic partnership grants program of NSERC, and in part by the NSERC postdoctoral fellowships program. The associate editor coordinating the review of this manuscript and approving it for publication was Prof. Athina P. Petropulu.

K. Zarifi is with the Institut National de la Recherche Scientifique-Énergie, Matériaux, et Télécommunications (INRS-EMT), Université du Québec and Concordia University, Montreal, QC H5A 1K6, Canada (e-mail: zarifi@ieee.org).

A. Ghrayeb is with the Department of Electrical and Computer Engineering, Concordia University, Montreal, QC H3G 1M8, Canada (e-mail: aghrayeb@ece.concordia.ca).

S. Affes is with the INRS-EMT, Université du Québec, Montreal, QC H5A 1K6, Canada (e-mail: affes@emt.inrs.ca).

Digital Object Identifier 10.1109/TSP.2009.2037065

a connected network such that a signal originating from any of them can eventually reach all others.[1]

When the DBF nodes cluster has a fixed topology, it may be reasonable to assume that the DBF nodes form a connected network. However, it is not always a well-justified assumption as optimizing the DBF performance frequently entails changing the topology of the DBF nodes cluster. For instance, as discussed above, it has been shown in [1]–[3] that the far-field beampattern heavily depends on the relative locations of the DBF nodes. In particular, when a WSN is comprised of uniformly distributed nodes on a large plane, the width of the average beampattern mainlobe is almost inversely proportional to the radius of the disc that includes the DBF nodes [1]. Therefore, as a principal aim in many beamforming applications is to generate a narrow mainlobe and a high beampattern directivity, the DBF nodes may have to be selected from an excessively large disc in the network. This, in turn, results in increasing the distances among the DBF nodes, and, consequently, increasing the probability that some of these nodes get disconnected from others. As a remedy, one may use the common approach of reestablishing the DBF nodes interconnections by means of using some idle nodes as relays. However, this can cause a substantial increase in the network energy consumption and the earlier depletion of the nodes' valuable energy resources.

A main contribution of this work is to show how nodes can be properly selected and used in DBF to simultaneously address the conflicting requirements of a high beampattern directivity and a strong network connectivity/high energy efficiency. Assuming that the WSN nodes are uniformly distributed on a large plane [1], [3], [14]–[17], we study the DBF technique in a general case where the DBF nodes are located on a ring of arbitrary inner and outer radii. While setting the ring inner radius to zero reduces our node selection region to the case considered in [1]–[3], we show how the ring inner and outer radii may be chosen differently than those in [1]–[3], not only to achieve the target average beampattern properties, but also to reduce the network energy waste and the DBF nodes disconnectivity probability. To this end, an average beampattern expression is derived for the case when the DBF nodes belong to an arbitrary ring. Then, given the ring outer radius, it is shown that the first null of the average beampattern is a decreasing function of the ring inner radius. This result is of particular practical importance as it shows that when the nodes are randomly located on a disc, the mainlobe of the average beampattern can be considerably shrunk just by letting the nodes in the inner parts of the disc remain in the sleeping mode to preserve energy while selecting the DBF nodes from a close vicinity of the disc perimeter. Similarly, given a target position of the first null of the average beampattern, it is also shown that the disc radius can be considerably reduced if the DBF nodes are selected from a narrow neighborhood close to the disc boundary.

The probability of having no isolated node is also obtained for two essential cases, namely, when the active nodes are selected from a large disc and when they are selected from a large narrow ring. Considering a large narrow ring and a disc with the same radius as the outer radius of the ring and assuming that both areas include the same number of active nodes, it is proved that the isolation probability of a node on the disc is much higher. It is further shown that when the nodes are selected from a disc, there are two approaches to reduce the node isolation probability: 1) Increasing the number of active nodes on the disc at the cost of a substantial increase in the network power consumption; and 2) reducing the disc radius at the expense of a considerable increase in the mainlobe width of the average beampattern.

Assuming that the DBF nodes are located on a large narrow ring, a simple approximate expression for the average beampattern is derived and then used to determine the null and the peak positions of the average beampattern as well as the peak values of its sidelobes. A tight lower bound on the average directivity of the beampattern is also derived. A simplified expression for this lower bound is offered and it is shown that the minimum rate at which the normalized directivity converges to unity is the same in both cases when the nodes are selected from a disc or from a narrow ring. However, when the nodes are selected from a disc, a large normalized directivity is associated with a substantial increase in the probability that the nodes lose interconnection.

When the number of DBF nodes is not large enough, the randomness of the nodes locations may cause a noticeable discrepancy between the average and a particular realization of the beampattern. For such scenarios, we derive an approximate complementary cumulative distribution function (CCDF) of the beampattern. Using the so-obtained CCDF, the probability that the beamformers' gain exceeds a given threshold can be evaluated at any arbitrary direction.

The proposed DBF technique is then extended to the case that the nodes are selected from multiple concentric rings. The average beampattern expression is derived for such a case and it is shown that if the rings radii are properly selected, the sidelobe peak levels can be substantially reduced. Finally, the case that the nodes' signals are contaminated by noise is studied. Considering an arbitrary noise correlation matrix, a SNR-optimal beamforming vector is derived and the associated average beampattern is obtained. It is shown that most properties of the average beampattern in the noise-free signal case carry over or can be directly extended to the noisy signal scenario.

The rest of the paper is organized as follows. Section II represents the proposed DBF technique and Section III analyzes the effects of the node selection region on the DBF performance. Section IV extends the proposed DBF technique to the multiple-ring scenario and Section V studies the noise-contaminated signal case. Simulation results are presented in Section VI and concluding remarks are given in Section VII.

II. Problem Formulation

A. Background

Consider a large WSN cluster whose nodes are uniformly distributed on $D(O, R_{\max})$, the disc centered at O with radius $R_{\max}$ [1], [14]–[17]. Let $S(O, R_{i,s}, R_{o,s})$ denote the ring centered at O with the inner radius $R_{i,s} \geq 0$ and the outer radius $R_{o,s} \leq R_{\max}$. It is assumed that $R_{i,s}$ and $R_{o,s}$ are selected such that $S(O, R_{i,s}, R_{o,s})$ has an area $A_S = \pi(R_{o,s}^2 - R_{i,s}^2)$

[1]In some cases, the nodes common signal may also be obtained by decoding the source transmitted signal. In such scenarios, the nodes connectivity should still be maintained for synchronization purposes.

large enough to include at least N nodes with a high probability. Note that as the nodes are uniformly distributed on a large plane, they are points of a homogenous two-dimensional Poisson process [14], [16]. Therefore, having at least N nodes on $S(O, R_{i,s}, R_{o,s})$ with a probability not less than ι requires that

$$\sum_{n=0}^{N-1} e^{-\rho A_S} \frac{(\rho A_S)^n}{n!} = \frac{\Gamma(N, \rho A_S)}{(N-1)!} \leq 1 - \iota \qquad (1)$$

where $\Gamma(\cdot,\cdot)$ is the incomplete Gamma function and ρ is the node density. Given ι, N, and ρ, the minimum feasible A_S can be obtained from (1). Selecting a ι close to one ensures the presence of at least N nodes on $S(O, R_{i,s}, R_{o,s})$ with a high probability. After N nodes are randomly selected from $S(O, R_{i,s}, R_{o,s})$, they share a common signal by means of, for instance, intercommunicating their sensed signals to distributively reach a consensus [10]–[12].[2] Then, $K \leq N$ members of the set participate in a DBF [1], [2] and collaboratively transmit their common signal aiming primarily to maximize the received power at the direction of AP located in the far-field of the plane containing $D(O, R_{\max})$. Optimal values of N and K depend on the application and all of our results hold for arbitrary N and $K \leq N$. However, it is instructive to overview the following guidelines on sensible choices of N and K.

- When the nodes "generate" their common signal by reaching a consensus, N should be large enough such that the reached consensus is a good approximation of the one that would be achieved if all cluster nodes joined in the consensus process. On the other hand, the number of internode transmissions required for nodes to reach a consensus typically shows a quadratic growth with respect to the number of nodes [10], [12]. Therefore, N should be selected as small as possible to avoid unnecessary internode transmissions. Note that the power consumption of a typical transceiver in the transmission/listening mode is three order of magnitude higher than its power consumption in the sleeping mode [18]. Therefore, when the N nodes are selected, all other nodes may be left in the sleeping mode to preserve energy.
- As the transmission range of a single node is typically far less than its distance to the AP, K should be large enough to substantially increase the nodes composite transmission range and keep the SNR at the AP above the required threshold. However, as nodes have independent clocks and do not share a common time reference, they should be synchronized prior to DBF [1], [4]. State of the art distributed synchronization algorithms require $2(K-1)$ serial internode transmissions to synchronize K nodes [13]. Therefore, an excessively large K not only results in an unnecessary network power depletion, but also may introduce an unacceptable delay in the communication process. Note that, one may alternatively use $K = N$ to avoid any possible system overhead that may be associated with the procedure of selecting K DBF nodes out of the N available nodes. However, this causes $N-K$ unnecessary nodes to participate in DBF instead of switching back to the sleeping mode and save energy. As discussed above, such a policy also increases the number of internode transmissions and the time required for synchronizing the DBF nodes.

The above discussion underlines the fact that one should refrain from choosing unnecessarily large N and K. Another important fact that follows from the above argument and will be further discussed in Section III-C is that the selected nodes have to extensively communicate with one another to gain access to a shared signal and synchronize prior to DBF. Therefore, these nodes should form a connected graph, and, in particular, none of them may be isolated: If the nodes transmission range is R_f, any selected node should have at least one other selected node in its R_f-neighborhood.

B. DBF Beampattern

The WSN cluster in a polar coordinate system is depicted in Fig. 1. Without loss of generality, we consider O as the pole and the line connecting O to the AP as the x-axis of the coordinate system. Let (r_k, ψ_k) and $B_0(Q, \phi_0 = 0)$ denote, respectively, the polar coordinates of the node k and the AP. We consider the case that the AP is in the far-field and, therefore, $Q \gg r_k$ and assume that the channels from all nodes to the AP are coherent [1]–[3], [9]. Let N nodes with random positions on $S(O, R_{i,s}, R_{o,s})$ share a zero-mean unit-variance signal $u(n)$ where n is the transmission slot index. Among them, $K \leq N$ nodes with the location vectors $\mathbf{r} = [r_1, r_2, \ldots, r_K]$ and $\boldsymbol{\psi} = [\psi_1, \psi_2, \ldots, \psi_K]$ synchronize and form a virtual antenna array to transmit $u(n)$ to the AP. It is noteworthy that as the channels from nodes to the AP are coherent, the signals received from all nodes at the AP have a similar quality. Therefore, the node selection procedure is substantially simplified as K nodes out of the N available nodes can be randomly selected to participate in DBF without causing any detrimental effect on the SNR at the AP. The base-band representation of the transmitted signal from the kth node in the nth transmission slot is $s_k(n) = w_k^* u(n)$ where w_k^* is the kth node beamforming weight. As the channels from all nodes to the AP are coherent, the base-band equivalent of the received signal from the kth node at an arbitrary point $B_\phi(Q, \phi)$ is [3]

$$y_{B_\phi,k}(n) = G d_{B_\phi,k}^{-\gamma/2} w_k^* u(n) e^{-j(2\pi/\lambda) d_{B_\phi,k}} \qquad (2)$$

where G is a constant that does not depend on the node index, $d_{B_\phi,k}$ is the Euclidian distance between the kth node and B_ϕ, while λ and γ are the carrier wavelength and the path loss exponent, respectively. Note that

$$\begin{aligned} d_{B_\phi,k} &= \left(Q^2 + r_k^2 - 2Q r_k \cos(\phi - \psi_k)\right)^{1/2} \\ &= \left((Q - r_k\cos(\phi-\psi_k))^2 + r_k^2(1-\cos^2(\phi-\psi_k))\right)^{1/2} \\ &\approx Q - r_k \cos(\phi - \psi_k) \end{aligned} \qquad (3)$$

where the approximation is due to the fact that $Q \gg r_k$. Using (3) in (2), we have

$$y_{B_\phi,k}(n) \approx G Q^{-\gamma/2} e^{-j(2\pi/\lambda)Q} u(n) w_k^* e^{j(2\pi/\lambda) r_k \cos(\phi - \psi_k)}. \qquad (4)$$

Introducing the steering vector towards ϕ as $\mathbf{a}_\phi \triangleq [e^{j(2\pi/\lambda) r_1 \cos(\phi-\psi_1)} \ \ldots \ e^{j(2\pi/\lambda) r_K \cos(\phi-\psi_K)}]^T$ and the

[2]The case that the sensor nodes only have access to noisy versions of the common signal is studied in details in Section V.

beamforming vector as $\mathbf{w} \triangleq [w_1 \ \dots \ w_K]^T$, the total received signal at B_ϕ due to all cluster nodes is approximately equal to

$$y_{B_\phi}(n) = GQ^{-\gamma/2} e^{-j(2\pi/\lambda)Q} u(n) \mathbf{w}^H \mathbf{a}_\phi. \tag{5}$$

Denoting the noise power at the AP by ϱ_0^2, the SNR at the AP can then be expressed as $\Omega = \varsigma \left|\mathbf{w}^H \mathbf{a}_0\right|^2 / \varrho_0^2$ where $\varsigma \triangleq |G|^2 Q^{-\gamma}$. Our goal is to find a $\mathbf{w}$ that maximizes Ω subject to the total power constraint $\|\mathbf{w}\|^2 \leq 1$. It is straightforward to show that the optimal beamforming vector is given by $\mathbf{w}_c = (1/\sqrt{K})\mathbf{a}_0$. Substituting $\mathbf{w}_c$ in (5) and using the definition of $\mathbf{a}_\phi$ to simplify the result, the received power at B_ϕ is then given by

$$\chi(\phi, \mathbf{r}, \boldsymbol{\psi}) = \varsigma K |F(\phi, \mathbf{r}, \boldsymbol{\psi})|^2 \tag{6}$$

where

$$\begin{aligned} F(\phi, \mathbf{r}, \boldsymbol{\psi}) &\triangleq \frac{1}{K} \sum_{k=1}^{K} e^{j(2\pi/\lambda) r_k (\cos(\psi_k) - \cos(\phi - \psi_k))} \\ &= \frac{1}{K} \sum_{k=1}^{K} e^{-j\beta(\phi) r_k \sin \tilde{\psi}_k} \end{aligned} \tag{7}$$

with $\beta(\phi) \triangleq (4\pi/\lambda)\sin(\phi/2)$ and $\tilde{\psi}_k \triangleq \psi_k - \phi/2$. $F(\phi, \mathbf{r}, \boldsymbol{\psi})$ is usually called the array factor at the direction ϕ [1]–[3]. Let R and Ψ denote, respectively, the random variable representing the distance of the selected nodes from the origin and the random variable representing the angular distance of the selected nodes from the x-axis minus $\phi/2$. Then, r_k and $\tilde{\psi}_k$ are realizations of R and Ψ, respectively. As the selected nodes are uniformly distributed on $S(O, R_{i,s}, R_{o,s})$, the probability density functions (PDFs) of R and Ψ are given by

$$\begin{aligned} f_R(r_k) &= \begin{cases} 2r_k A_S^{-1}, & r_k \in [R_{i,s}, R_{o,s}] \\ 0, & \text{elsewhere} \end{cases} \\ f_\Psi(\tilde{\psi}_k) &= \frac{1}{2\pi} \quad \psi \in [-\pi, \pi). \end{aligned} \tag{8}$$

For the random variables R and Ψ with the PDFs given in (8), it is shown in Theorem 5 in Appendix A that the PDF of $Z \triangleq R \sin \Psi$ is equal to $f_Z(z)$ in (9), shown at the bottom of the page. Let $z_k \triangleq r_k \sin \tilde{\psi}_k$. It follows from the above discussion that (6) can be equivalently represented as $\check{\chi}(\phi, \mathbf{z}) = \varsigma K |\check{F}(\phi, \mathbf{z})|^2$ where

$$\check{F}(\phi, \mathbf{z}) = \frac{1}{K} \sum_{k=1}^{K} e^{-j\beta(\phi) z_k} \tag{10}$$

is an alternative representation of the array factor (7) and $\mathbf{z} \triangleq [z_1, z_2, \dots, z_K]$ is a realization of a K-dimensional random vector $\mathbb{Z} = [Z_1, Z_2, \dots, Z_K]$ with independent entries that are identically distributed according to (9). Let us define

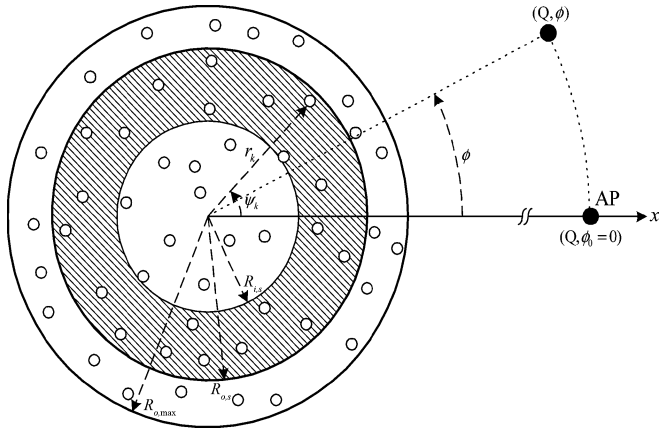

Fig. 1. The WSN cluster in a polar coordinate system.

the far-field beampattern as the received power from the WSN cluster normalized by ςK, that is, $P(\phi, \mathbf{z}) \triangleq \check{\chi}(\phi, \mathbf{z})/\varsigma K$. We then have

$$\begin{aligned} P(\phi, \mathbf{z}) &= |\check{F}(\phi, \mathbf{z})|^2 \\ &= \frac{1}{K} + \frac{1}{K^2} \sum_{k=1}^{K} e^{-j\beta(\phi) z_k} \sum_{l=1 l \neq k}^{K} e^{j\beta(\phi) z_l}. \end{aligned} \tag{11}$$

The far-field beampattern is an essential feature of a beamformer as it represents (a normalized version of) the spatial distribution of the impinging power from the beamformer and, therefore, not only its level at $\phi_0 = 0$ is proportional to the SNR at the AP, but also determines the level of interference inflicted on unintended receivers at any arbitrary angular direction $\phi \neq 0$. In this work, $P(\phi, \mathbf{z})$ is a random variable that depends on the realization of $\mathbb{Z}$. This justifies the practical value of the study of $P_{\text{av}}(\phi) \triangleq \mathrm{E}_{\mathbb{Z}} \{P(\phi, \mathbb{Z})\}$. Note also that as the entries of $\mathbb{Z}$ are independent random variables, it is direct to apply the strong law of large numbers when $K \rightarrow \infty$ to show that any arbitrary realization of $P(\phi, \mathbb{Z})$ converges with probability one to $P_{\text{av}}(\phi)$. It can be inferred from the above fact that, when K is large enough, the difference between $P_{\text{av}}(\phi)$ and $P(\phi, \mathbf{z})$ is negligible at all directions (see [1] for a similar observation). This further substantiates the practical importance of $P_{\text{av}}(\phi)$.

III. The Effects of the Node Selection Region on the DBF Performance

It is proven in Theorem 6 in Appendix A that, if a random variable Z is distributed according to (9), we have

$$\begin{aligned} \mathrm{E}\left\{e^{j\beta(\phi)Z}\right\} &= \frac{2}{R_{o,s}^2 - R_{i,s}^2} \\ &\times \left(\frac{R_{o,s}}{\beta(\phi)} J_1 \left(R_{o,s}\beta(\phi)\right) - \frac{R_{i,s}}{\beta(\phi)} J_1 \left(R_{i,s}\beta(\phi)\right) \right) \end{aligned} \tag{12}$$

$$f_Z(z) = \begin{cases} 2A_S^{-1} \left(R_{o,s} \sqrt{1 - \left(\frac{z}{R_{o,s}}\right)^2} - R_{i,s} \sqrt{1 - \left(\frac{z}{R_{i,s}}\right)^2} \right) & 0 \leq |z| < R_{i,s} \\ 2A_S^{-1} R_{o,s} \sqrt{1 - \left(\frac{z}{R_{o,s}}\right)^2} & R_{i,s} \leq |z| \leq R_{o,s} \end{cases} \tag{9}$$

$$P_{\rm av}(\phi) = \frac{1}{K} + \left(1 - \frac{1}{K}\right) \left| \mathrm{E}\left\{ e^{j\beta(\phi)Z} \right\} \right|^2$$
$$= \frac{1}{K} + \left(1 - \frac{1}{K}\right) \left| \frac{2}{R_{o,s}^2 - R_{i,s}^2} \cdot \left(\frac{R_{o,s}}{\beta(\phi)} J_1\left(R_{o,s}\beta(\phi)\right) - \frac{R_{i,s}}{\beta(\phi)} J_1\left(R_{i,s}\beta(\phi)\right) \right) \right|^2 \quad (13)$$

where $J_n(\cdot)$ is the nth order Bessel function of the first kind. Using (12) and the fact that the entries of $\mathbb{Z}$ are independently distributed, it is direct to show that (13), shown at the top of the page holds. It is noteworthy that when $R_{i,s} = 0$, that is, when the ring $S(O, R_{i,s}, R_{o,s})$ transforms to $D(O, R_{o,s})$, the disc centered at O with radius $R_{o,s}$, (13) simplifies to

$$P_{\rm av}(\phi) = \frac{1}{K} + \left(1 - \frac{1}{K}\right) \left| 2 \cdot \frac{J_1\left(R_{o,s}\beta(\phi)\right)}{R_{o,s}\beta(\phi)} \right|^2. \quad (14)$$

The same expression as in (14) has been obtained for $P_{\rm av}(\phi)$ in [1] that exclusively considers the special scenario of $R_{i,s} = 0$. In Sections III-A–III-E, we analyze $P_{\rm av}(\phi)$ in (13) and explore some advantages of choosing $R_{i,s} \neq 0$ with respect to the conventional approach of [1] that selects the nodes from $D(O, R_{o,s})$.

A. The Mainlobe of the Average Beampattern

Similar to the beamforming for centralized antenna arrays, it is crucial to form a beampattern with a narrow mainlobe when using DBF. A narrow mainlobe implies that most of the transmitted power concentrates in the direction of the target AP. Moreover, when the target AP has a small angular distance from other receivers such as other clusters' APs, a narrow mainlobe is essential to avoid inducing significant interference on the unintended receiving terminals. In particular, it is advisable in the latter case to have the mainlobe narrow enough such that the first null of the beampattern $P(\phi, \mathbb{Z})$ positions in the direction of the unintended receiver with the smallest angular distance from the target AP. It is noteworthy that, as $P(\phi, \mathbb{Z})$ is a random variable, the positions of its nulls are also random quantities. However, as discussed at the end of Section II-B, when K is large enough, all realizations of $P(\phi, \mathbb{Z})$ are close to $P_{\rm av}(\phi)$, and, therefore, the position of the first null of $P_{\rm av}(\phi)$ (in the sense of the second term in (13)) is a reliable approximation of that of the first null of $P(\phi, \mathbb{Z})$ for any arbitrary realization of $\mathbb{Z}$.

As can be observed from (12) and (13), the position of the ith null of $P_{\rm av}(\phi)$ coincides with $\phi_{(n),i}$, the ith positive root of $\mathrm{E}\{e^{j\beta(\phi)Z}\}$. In what follows, we analyze $\phi_{(n),1}$ as a function of $\alpha \triangleq R_{i,s}/R_{o,s}$. First, let us introduce

$$f(x, \alpha) \triangleq \frac{2}{1 - \alpha^2} \left(\frac{J_1(x)}{x} - \frac{\alpha J_1(\alpha x)}{x} \right), \quad 0 \leq \alpha < 1. \quad (15)$$

From (12), we have $\mathrm{E}\{e^{j\beta(\phi)Z}\} = f(R_{o,s}\beta(\phi), \alpha)$. The following theorem holds.

Theorem 1: Let $x^*(\alpha)$ be the smallest positive number such that $f(x^*(\alpha), \alpha) = 0$. We have

$$x^*(0) = \nu_1 \quad (16)$$
$$\lim_{\alpha \longrightarrow 1^-} x^*(\alpha) = \nu_0 \quad (17)$$

where $\nu_1 \approx 3.8317$ and $\nu_0 \approx 2.4048$ are the first positive roots of $J_1(x)$ and $J_0(x)$, respectively. For any $\alpha \in (0, 1)$

$$\nu_0 < x^*(\alpha) < \nu_1. \quad (18)$$

Moreover, $x^*(\alpha)$ is the only root of $f(x, \alpha)$ in (ν_0, ν_1) and

$$\frac{dx^*(\alpha)}{d\alpha} < 0. \quad (19)$$

Proof: See Appendix B.

Theorem 1 shows that, for any given $R_{o,s}$, $\phi_{(n),1}$ is a decreasing function of $R_{i,s}$: If $R_{i,s} = 0$, or, equivalently, $\alpha = 0$, (16) indicates that $R_{o,s}\beta(\phi_{(n),1}) = \nu_1$, or, in other words

$$\phi_{(n),1} = 2\arcsin\left((4\pi R_{o,s})^{-1}\lambda\nu_1\right), \quad \alpha = 0. \quad (20)$$

Meanwhile, increasing $R_{i,s}$ results in increasing α, which, according to (19), decreases $\phi_{(n),1}$. The steady decrease in $\phi_{(n),1}$ continues until $R_{i,s}$ approaches $R_{o,s}$, or, in other words, $\alpha \approx 1$. In such a case, as shown in (17), $R_{o,s}\beta(\phi_{(n),1}) \approx \nu_0$. This means that

$$\phi_{(n),1} \approx 2\arcsin\left((4\pi R_{o,s})^{-1}\lambda\nu_0\right), \quad \alpha \approx 1. \quad (21)$$

Note from (21) that, a narrow mainlobe, or, equivalently, a small $\phi_{(n),1}$, requires having a large $R_{o,s}$. This implies that $R_{i,s}$ may be very close to $R_{o,s}$ in practice without making $A_S = \pi(R_{o,s}^2 - R_{i,s}^2)$ so small that the number of nodes on $S(O, R_{i,s}, R_{o,s})$ drops below N. In other words, $S(O, R_{i,s}, R_{o,s})$ can be a narrow ring but large enough to include at least N nodes.

It follows from (20) and (21) that, when $R_{o,s}/\lambda$ is large, $\phi_{(n),1} \approx (2\pi R_{o,s})^{-1}\lambda\nu_1$ for $R_{i,s} = 0$ while $\phi_{(n),1} \approx (2\pi R_{o,s})^{-1}\lambda\nu_0$ for $R_{i,s} \approx R_{o,s}$. The following results are directly obtained from the above observation.

- Since $\nu_1 \approx 3.8317$ and $\nu_0 \approx 2.4048$, the first null of $P_{\rm av}(\phi)$ can be reduced by up to 37% when increasing $R_{i,s}$ from zero to a close proximity of $R_{o,s}$. Interestingly, this means that it is possible to considerably shrink the mainlobe of $P_{\rm av}(\phi)$ just by selecting the active nodes from a close vicinity of the perimeter of $D(O, R_{o,s})$ while leaving all other nodes in the sleeping mode to preserve energy.
- Without having any effect on the target $\phi_{(n),1}$, the outer radius of S can be reduced from $R_{o,s} \approx (2\pi\phi_{(n),1})^{-1}\lambda\nu_1$ to $R_{o,s} \approx (2\pi\phi_{(n),1})^{-1}\lambda\nu_0$, just by increasing the inner radius $R_{i,s}$ from zero to $R_{i,s} \approx R_{o,s} \approx (2\pi\phi_{(n),1})^{-1}\lambda\nu_0$. This property can be very useful when $R_{\max}$ is smaller than $(2\pi\phi_{(n),1})^{-1}\lambda\nu_1$.

B. The Network Energy

As discussed above, all the nodes on $D(O, R_{i,s})$ as well as the unselected nodes from $S(O, R_{i,s}, R_{o,s})$ are used neither in DBF nor in the preliminary step of generating the common signal using, for instance, a consensus process. Therefore, they may be left in the sleeping mode. Note that, a node using a typical

transceiver with the transmission range of several tens of meters has a power consumption in the order of 10 mW in the transmission/listening mode while having a power consumption in the order of 10 μW in the sleeping mode [18]. Moreover, as pointed out in Section II-A, the number of the internode transmissions required to reach a consensus is typically proportional to N^2 [10]. Therefore, even if one extra node, say, from $D(O, R_{i,s})$, decides to join the consensus process, the total number of required internode transmissions may considerably increase. As such, the technique proposed here tends to save a substantial amount of energy as compared to the technique presented in [1] that does not propose a policy to switch off any cluster nodes.

As an alternative to select the nodes from $S(O, R_{i,s}, R_{o,s})$, one may randomly choose N nodes from $D(O, R_{o,s})$ to reach a consensus, while leaving all other nodes in the sleeping mode. After the consensus is reached, K nodes are delegated to perform DBF. Although such an approach increases $\phi_{(n),1}$ to its maximum value of $2\arcsin\left((4\pi R_{o,s})^{-1}\lambda\nu_1\right)$, one may argue that, as far as the energy saving is concerned, it is immaterial whether the N active nodes are selected from $S(O, R_{i,s}, R_{o,s})$ or from $D(O, R_{o,s})$. As will be shown in Section III-C, this is not a correct argument in general as direct internode communications may be hampered when the active nodes are distributed throughout the larger area of $D(O, R_{o,s})$.

C. The Network Connectivity

As discussed in Sections II-A and III-B, the selected nodes should form a connected network in the sense that a message originating from any node should be able to diffuse throughout the whole network. There is a rich literature [14], [15], [19], [20] indicating that the connectivity analysis is a nontrivial problem even in an asymptotic regime of infinite-size homogenous network. This problem is more severe in our context due to the facts that the number of selected nodes is finite and, moreover, boundary conditions are involved as the nodes may be selected from a narrow ring. Therefore, we approach the above problem by establishing a necessary condition for the network connectivity in the cases of our special interest. In particular, in view of the fact that the absence of isolated nodes (the nodes that do not have any other nodes in their transmission range) is a necessary condition for the connectivity of a network, we derive the probability of having no isolated nodes for two essential cases when the nodes are selected from a large disc and when they are selected from a large narrow ring. Note that, the above probability is an upper bound on the probability of the network connectivity, and, as shown in [14], [15], [20], this bound is very tight when the N nodes are selected from a large disc. The following theorem is fundamental for our later developments.

Theorem 2: Assume that the nodes transmission range is R_f. If the nodes are uniformly distributed on a ring $S(O, R_{i,s}, R_{o,s})$ where

$$0.5\,(R_{o,s} - R_{i,s}) \ll R_f \ll R_{o,s} \tag{22}$$

then the probability that the distance of two arbitrarily selected nodes[3] is not greater than R_f is

$$P^{(s)} \approx \frac{1}{\pi} \cdot \frac{R_f}{R_{o,s}}. \tag{23}$$

In turn, if the nodes are uniformly distributed on a disc $D(O, R_{o,d})$ where $R_f \ll R_{o,d}$ then the probability that the distance of two arbitrarily selected nodes is not greater than R_f is

$$P^{(d)} \approx \frac{R_f^2}{R_{o,d}^2}. \tag{24}$$

Proof: See Appendix C.

Before proceeding to further developments, we would like to stress that (22) is a practical assumption implying that $S(O, R_{i,s}, R_{o,s})$ is a large narrow ring. In fact, if A_S is kept fixed, $R_{o,s}$ can always be chosen large enough such that both inequalities of (22) hold true. The following example is also helpful to verify the feasibility of (22) in practical scenarios.

1) Example 1: Consider the case that the node density is $\rho = 0.1\ \mathrm{m}^{-2}$, $R_f = 20$ m, $R_{o,s} = 200\ \mathrm{m} \gg R_f$, and we aim to determine $R_{i,s}$ such that at least $N = 200$ nodes are on $S(O, R_{i,s}, R_{o,s})$ with a probability not less than $\iota = 1 - 10^{-4}$. Using (1), it is direct to show that an inner radius as large as $R_{i,s} = 198.2$ m satisfies the above requirement.

It is interesting to observe from Theorem 2 that $P^{(s)}$ decreases with a rate inversely proportional to $R_{o,s}$, while $P^{(d)}$ decreases with a much faster rate that is inversely proportional to $R_{o,d}^2$. From Theorem 2, it also follows that $\Pr\{\text{a node is not isolated}\} = 1 - \left(1 - P^{(\bullet)}\right)^{N-1}$ where $\bullet$ is either s or d depending on the region from which the N nodes are selected. Note also that, when N is large, the isolation of different nodes can be considered as almost independent events [20]. As such, the probability of having no isolated nodes is given by

$$P_{\bar{I}}^{(\bullet)} \approx \left(1 - \left(1 - P^{(\bullet)}\right)^{N-1}\right)^N. \tag{25}$$

2) Example 2: Consider the parameters of Example 1. Using (23) in (25), it follows that $P_{\bar{I}}^{(s)} \approx 0.9996$. As such, it is extremely unlikely that any of the 200 nodes selected from $S(O, 198.2\ \mathrm{m}, 200\ \mathrm{m})$ are isolated. Note that, if $N = 200$ nodes are selected from $D(O, 200\ \mathrm{m})$, then, it follows from (24) and (25) that $P_{\bar{I}}^{(d)} = \mathcal{O}(10^{-13})$, and, therefore, it is almost sure that at least one selected node is isolated, and, hence, the network is disconnected. In fact, it can be shown from (25) that at least $N = 1500$ nodes have to be selected from $D(O, 200\ \mathrm{m})$ to reach the target $P_{\bar{I}}^{(d)} = 0.9996$. Note that, reaching such a target $P_{\bar{I}}^{(d)}$ comes at the price of a substantial increase in the network power waste due to 650% increase in the number of active nodes.

As can be observed from (24) and (25), the only means to increase $P_{\bar{I}}^{(d)}$ without requiring to activate extra nodes is to decrease $R_{o,d}$. In fact, it can be shown from (23), (24), and (25) that, if the number of active nodes in both $S(O, R_{i,s}, R_{o,s})$ and $D(O, R_{o,d})$ are the same, then $P_{\bar{I}}^{(d)}$ and $P_{\bar{I}}^{(s)}$ are approximately equal when

$$R_{o,d} = \sqrt{\pi R_f R_{o,s}}. \tag{26}$$

Taking into account the assumption that $R_f \ll R_{o,s}$, (26) shows that $R_{o,d}$ should be considerably less than $R_{o,s}$. According to (20) and (21), this, in turn, means that the width of the resulting average beampattern mainlobe becomes considerably larger than that of the average beampattern mainlobe when the nodes are chosen from $S(O, R_{i,s}, R_{o,s})$.

[3]It is assumed that $N \geq 2$ and, therefore, the distance between the selected nodes is well-defined.

$$
\begin{aligned}
P_{\rm av}(\phi) &\approx \lim_{R_{i,s}\longrightarrow R_{o,s}} \left(\frac{1}{K}+\left(1-\frac{1}{K}\right)\left|\frac{2}{R_{o,s}^2-R_{i,s}^2}\left(\frac{R_{o,s}}{\beta(\phi)}J_1\left(R_{o,s}\beta(\phi)\right)-\frac{R_{i,s}}{\beta(\phi)}J_1\left(R_{i,s}\beta(\phi)\right)\right)\right|^2\right)\\
&=\frac{1}{K}+\left(1-\frac{1}{K}\right)\left|\frac{1}{R_{o,s}\beta(\phi)}\lim_{R_{i,s}\longrightarrow R_{o,s}}\frac{R_{o,s}\beta(\phi)J_1\left(R_{o,s}\beta(\phi)\right)-R_{i,s}\beta(\phi)J_1\left(R_{i,s}\beta(\phi)\right)}{R_{o,s}\beta(\phi)-R_{i,s}\beta(\phi)}\right|^2\\
&=\frac{1}{K}+\left(1-\frac{1}{K}\right)\left|\frac{1}{R_{o,s}\beta(\phi)}\cdot\frac{\partial\left(R_{o,s}\beta(\phi)J_1\left(R_{o,s}\beta(\phi)\right)\right)}{\partial\left(R_{o,s}\beta(\phi)\right)}\right|^2\\
&=\frac{1}{K}+\left(1-\frac{1}{K}\right)\left|J_0(R_{o,s}\beta(\phi))\right|^2
\end{aligned}
\tag{27}
$$

Our results in this subsection may be summarized as follows: Consider a large narrow ring and a disc with the same radius as the outer radius of the ring. If the number of active nodes on the ring and the disc are equal, then the probability that some nodes on the disc are isolated is much higher. There are two approaches to reduce this probability: 1) Increasing the number of active nodes on the disc at the cost of a substantial increase in the network power consumption; and 2) reducing the disc radius in exchange to a considerable increase in the width of the average beampattern mainlobe.

D. Approximate Average Beampattern

As discussed in Section III-A, the practical interest in forming a narrow mainlobe necessitates $\phi_{(n),1}$ to be small. According to the developments in the same subsection, $\phi_{(n),1}$ is inversely proportional to $R_{o,s}$. Therefore, a narrow mainlobe can be in fact associated with a large $R_{o,s}$. At the same time, following our results in the network energy preservation and the network connectivity in Sections III-B and III-C, it may be preferable to choose $A_S=\pi R_{o,s}^2-\pi R_{i,s}^2$ just large enough to make sure that $S(O,R_{i,s},R_{o,s})$ includes N nodes. As discussed after Theorem 2, it is direct to show that increasing $R_{o,s}$ while keeping A_S fixed results in an $R_{i,s}$ that is close to $R_{o,s}$, or, equivalently, a large narrow ring $S(O,R_{i,s},R_{o,s})$. For such a scenario, $P_{\rm av}(\phi)$ in (13) can be approximated as shown by (27) at the top of the page. Using the fact that

$$
J_0(x)\approx\sqrt{\frac{2}{\pi x}}\cos\left(x-\frac{\pi}{4}\right)\quad x\gg\frac{1}{4} \tag{28}
$$

$P_{\rm av}(\phi)$ in (27) can be further simplified to

$$
P_{\rm av}(\phi)\approx\frac{1}{K}+\left(1-\frac{1}{K}\right)\frac{2}{\pi R_{o,s}\beta(\phi)}\cos^2\left(R_{o,s}\beta(\phi)-\frac{\pi}{4}\right) \tag{29}
$$

for $R_{o,s}\beta(\phi)\gg 1/4$. Let $\phi_{(n),l}$ and $\phi_{(p),l}$ denote the lth null and the lth peak positions of the average beampattern, respectively (note that $\phi_{(p),0}=\phi_0=0$). It follows from (29) that

$$
\begin{aligned}
\phi_{(n),l}&\approx 2\arcsin\left(\frac{\lambda\left(l-\frac{1}{4}\right)}{4R_{o,s}}\right)\\
\phi_{(p),l}&\approx 2\arcsin\left(\frac{\lambda\left(l+\frac{1}{4}\right)}{4R_{o,s}}\right)
\end{aligned}
\tag{30}
$$

for $l=1,2,\ldots$. It is noteworthy that the approximate $\phi_{(n),1}$ obtained from (30) is in fact very close to the approximate $\phi_{(n),1}$ derived in (21). Note also that, the approximations in (30) provide a simple technique to derive $R_{o,s}$ and $R_{i,s}$: Given a desired $\phi_{(n),l}$ or $\phi_{(p),l}$, one may determine the required $R_{o,s}$ from (30), and, then, use the preassigned $A_S=\pi R_{o,s}^2-\pi R_{i,s}^2$ to obtain $R_{i,s}$. We also obtain from (29) and (30) that the lth peak of the average sidelobe is approximately given by

$$
P_{\rm av}(\phi_{(p),l})\approx\frac{1}{K}+\left(1-\frac{1}{K}\right)\frac{2}{\pi^2\left(l+\frac{1}{4}\right)}. \tag{31}
$$

Similar to the case where the nodes are selected from a disc [1], it follows from (31) that $P_{\rm av}(\phi_{(p),l})$ only loosely depend on K while being completely independent from $R_{o,s}$. As such, it is not possible to effectively reduce the sidelobe peak levels in either case that the nodes are selected from a disc or the case that they are chosen from a narrow ring. To get around this problem, it has been suggested in [1] to increase the disc radius aiming to position most of the major sidelobe peaks around $\phi_0=0$. As can be observed from (30), the same technique may be used when the nodes are selected from $S(O,R_{i,s},R_{o,s})$. However, in the scenarios where unintended receivers are in a small angular spread around the target AP, having multiple large sidelobe peaks concentrated in a close vicinity of $\phi_0=0$ may result in inflicting considerable interfering power on these receivers. Note that, this interfering effect can be more significant when the nodes are selected from a narrow ring as, in such a case, the sidelobe peak levels of the average beampattern diminish with a relatively low rate that is proportional to their index number. Section IV presents a technique to effectively tackle the above problem. In particular, it will be shown that $P_{\rm av}(\phi_{(p),l})$ can be significantly reduced if the node selection region is expanded to multiple concentric rings of proper sizes.

E. Average Directivity

Average directivity [1], [2]

$$
D_{\rm av}\triangleq{\rm E}_{\mathbb{Z}}\left\{\frac{\int_{-\pi}^{\pi}P(0,\mathbb{Z})d\phi}{\int_{-\pi}^{\pi}P(\phi,\mathbb{Z})d\phi}\right\}={\rm E}_{\mathbb{Z}}\left\{\frac{2\pi}{\int_{-\pi}^{\pi}P(\phi,\mathbb{Z})d\phi}\right\} \tag{32}
$$

is a parameter that measures the beamforming efficiency to concentrate the transmitted power towards the desired direction. Similar to [1], [2], $D_{\rm av}$ in (32) cannot be computed in a closed form. However, following Jensen's inequality, it is direct to show that [1]

$$
D_{\rm av}\geq\tilde{D}_{\rm av}\triangleq\frac{2\pi}{{\rm E}_{\mathbb{Z}}\left\{\int_{-\pi}^{\pi}P(\phi,\mathbb{Z})d\phi\right\}}=\frac{2\pi}{\int_{-\pi}^{\pi}P_{\rm av}(\phi)d\phi}. \tag{33}
$$

Recalling the fact that $\lim_{K\longrightarrow\infty}P(\phi,\mathbb{Z})=P_{\rm av}(\phi)$ for any ϕ and any realization of $\mathbb{Z}$, it is expected that $\lim_{K\longrightarrow\infty}D_{\rm av}=\tilde{D}_{\rm av}$. This implies that $\tilde{D}_{\rm av}$ is a tight lower-bound on $D_{\rm av}$ for large values of K. The following theorem derives lower-bounds

on the average directivity in terms of K and $R_{o,s}/\lambda$ in the case that the nodes are selected from a large narrow ring.

Theorem 3: If (27) holds, we have

$$\frac{\tilde{D}_{\rm av}}{K} \approx \frac{1}{1+(K-1)\,{}_2F_3\left(\frac{1}{2},\frac{1}{2};1,1,1,-\left(\frac{4\pi R_{o,s}}{\lambda}\right)^2\right)} \quad (34)$$

where ${}_2F_3\left(1/2,1/2;1,1,1,-(4\pi R_{o,s}/\lambda)^2\right)$ is a generalized hypergeometric function. Moreover, it holds for large $R_{o,s}/\lambda$ that

$$\frac{D_{\rm av}}{K} \geq \frac{1}{1+(K-1)\frac{\pi^2+4\ln\left(\frac{16R_{o,s}}{\lambda}\right)}{\frac{4\pi^3 R_{o,s}}{\lambda}}}. \quad (35)$$

Proof: See Appendix D.

Note that $\lim_{x\longrightarrow\infty}\ {}_2F_3\left(1/2,1/2;1,1,1,-x^2\right) = 0$. Therefore, as $R_{o,s}/\lambda$ grows, the normalized average directivity converges to its maximum value of 1. The convergence rate is more visible from (35) which indicates that

$$\frac{D_{\rm av}}{K} \geq \frac{1}{1+\mathcal{O}\left(\frac{K}{\frac{R_{o,s}}{\lambda}}\right)} \quad (36)$$

for large K and $R_{o,s}/\lambda$. An inequality similar to (36) has been obtained in [1], (33), for the case that the nodes are selected from $D(O,R_{o,s})$. Comparing (36) with its counterpart inequality in [1], it follows that the minimum rate at which the normalized directivity converges to unity is the same in both cases that the nodes are selected from a disc and from a narrow ring. However, while in either case $(K/R_{o,s})/\lambda$ should be small to have a normalized directivity close to unity, when the nodes are selected from a disc, a small $(K/R_{o,s})/\lambda$ necessitates having K nodes scattered throughout a disc with a large area of $\pi R_{o,s}^2$. This, in turn, substantially increases the probability that the nodes lose interconnection (see Section III-C). In contrast, if the nodes are selected from a narrow ring, $R_{i,s}$ and $R_{o,s}$ may be chosen such that $(K/R_{o,s})/\lambda$ is arbitrarily small while keeping $A_S = \pi(R_{o,s}^2 - R_{i,s}^2)$ fixed. As discussed in Section III-C, this ameliorates the problem of lack of network connectivity when $R_{o,s}$ grows.

F. Statistical Analysis of the Beampattern

When K is not large enough, the realizations of $P(\phi,\mathbb{Z})$ may be noticeably different from $P_{\rm av}(\phi)$ specially in the sidelobes region [1]. In such scenarios, the technique presented in [1, Sec. IV-A] can be directly applied to numerically compute the CCDF of $P(\phi,\mathbb{Z})$ at any arbitrary direction ϕ. In view of the fact that $\check{F}(\phi,\mathbb{Z})$ is the sum of K independent identically distributed (i.i.d.) random variables (see (10)), a more analytically tractable alternative technique to evaluate the CCDF of $P(\phi,\mathbb{Z})$ is to use the central limit theorem and approximate the distribution of $\check{F}(\phi,\mathbb{Z})$ by that of a complex Gaussian random variable. The so-obtained approximate distribution may then be used to derive an approximate CCDF of $P(\phi,\mathbb{Z})$ [1]. Following the latter approach, let us represent $\check{F}(\phi,\mathbb{Z}) = (1/\sqrt{K})\cdot(X-jY)$ where $X \triangleq (1/\sqrt{K})\cdot\sum_{k=1}^{K}\cos(\beta(\phi)Z_k)$ and $Y \triangleq (1/\sqrt{K})\cdot\sum_{k=1}^{K}\sin(\beta(\phi)Z_k)$. To obtain the Gaussian approximate of the joint distribution of X and Y, it is required to derive the first and the second moments of the latter two random variables. Using (9), it can be readily proved that $\mathrm{E}\{Y\} = \mathrm{E}\{XY\} = 0$, while

$$\begin{aligned}
\mathrm{E}\{X\} &= \sqrt{K}\left(\frac{2R_{o,s}J_1\left(R_{o,s}\beta(\phi)\right) - 2R_{i,s}J_1\left(R_{i,s}\beta(\phi)\right)}{R_{o,s}^2\beta(\phi) - R_{i,s}^2\beta(\phi)}\right)\\
\sigma_X^2 &= \frac{1}{2} + \frac{R_{o,s}J_1\left(2R_{o,s}\beta(\phi)\right) - R_{i,s}J_1\left(2R_{i,s}\beta(\phi)\right)}{2R_{o,s}^2\beta(\phi) - 2R_{i,s}^2\beta(\phi)}\\
&\quad - \left(\frac{2R_{o,s}J_1\left(R_{o,s}\beta(\phi)\right) - 2R_{i,s}J_1\left(R_{i,s}\beta(\phi)\right)}{R_{o,s}^2\beta(\phi) - R_{i,s}^2\beta(\phi)}\right)^2\\
\sigma_Y^2 &= \frac{1}{2} - \frac{R_{o,s}J_1\left(2R_{o,s}\beta(\phi)\right) - R_{i,s}J_1\left(2R_{i,s}\beta(\phi)\right)}{2R_{o,s}^2\beta(\phi) - 2R_{i,s}^2\beta(\phi)}.
\end{aligned} \quad (37)$$

Note that when the nodes are selected from a large narrow ring, a similar approach as in (27) may be applied to show that

$$\begin{aligned}
\mathrm{E}\{X\} &\approx \sqrt{K}J_0\left(R_{o,s}\beta(\phi)\right)\\
\sigma_X^2 &\approx \frac{1}{2} + \frac{1}{2}J_0\left(2R_{o,s}\beta(\phi)\right) - J_0^2\left(R_{o,s}\beta(\phi)\right)\\
\sigma_Y^2 &\approx \frac{1}{2} - \frac{1}{2}J_0\left(2R_{o,s}\beta(\phi)\right).
\end{aligned} \quad (38)$$

The joint PDF of X and Y can then be computed as

$$f_{X,Y}(x,y) = \frac{1}{2\pi\sigma_X\sigma_Y}\exp\left(-\frac{|x-\mathrm{E}\{X\}|^2}{2\sigma_X^2} - \frac{y^2}{\sigma_Y^2}\right). \quad (39)$$

Therefore, the CCDF of $P(\phi,\mathbb{Z})$ at κ is given by

$$\begin{aligned}
\Pr\left[P(\phi,\mathbb{Z}) > \kappa\right] &= \Pr\left[|\check{F}(\phi,\mathbb{Z})|^2 > \kappa\right]\\
&= \Pr\left[X^2+Y^2 > K\kappa\right]\\
&= \int_{\sqrt{K\kappa}}^{\infty}\int_{-\pi}^{\pi} r f_{X,Y}\\
&\quad \times (r\cos\omega, r\sin\omega)d\omega dr.
\end{aligned} \quad (40)$$

In general, (40) may be efficiently computed using numerical integration. However, if $R_{i,s}\beta(\phi)$ is large, we have from (37) (or (38)) that $\sigma_X^2 \approx \sigma_Y^2 \approx 1/2$. In such a case, (40) simplifies to

$$\Pr\left[P(\phi,\mathbb{Z}) > \kappa\right] = Q_1\left(\sqrt{2}m_X, \sqrt{2K\kappa}\right). \quad (41)$$

where $Q_1(\cdot,\cdot)$ is the first-order Marcum-Q function. Finally, if $R_{i,s}\beta(\phi)$ is large enough such that $\mathrm{E}\{X\} \approx 0$, then

$$\Pr\left[P(\phi,\mathbb{Z}) > \kappa\right] = e^{-K\kappa}. \quad (42)$$

Note that similar results as in (41) and (42) have been obtained before in [1] in the case that the nodes are selected from $D(O,R_{o,s})$ with $R_{o,s}\beta(\phi) \gg 1$.

IV. Extension to Multiple Concentric Rings

As can be observed from (31), when $R_{i,s} \approx R_{o,s}$, the first and the largest sidelobe peak of the average beampattern is given by $P_{\rm av}(\phi_{(p),l}) \approx 0.16 + 0.84/K$ which is around 8 dB less than the mainlobe maximum value. In applications that such a sidelobe peak level is not acceptable, the DBF nodes may be selected from multiple concentric rings of proper radii to reduce the sidelobe peak value. To show this, let us assume that the K nodes used in DBF are randomly selected from M concentric rings

$S_m(O, R_{i,s}^{(m)}, R_{o,s}^{(m)})$, $m = 1, \ldots, M$ where $R_{o,s}^{(m)} \leq R_{i,s}^{(m+1)}$. Similar to the single-ring case, it can be shown that

$$P_{\text{av}}(\phi) = \frac{1}{K} + \left(1 - \frac{1}{K}\right) \left| \text{E}\left\{ e^{j\beta(\phi)Z} \right\} \right|^2 \tag{43}$$

where, as proven in Appendix A, (44), shown at the bottom of the page, holds. Assume that $A_{S_m} = \pi {R_{o,s}^{(m)}}^2 - \pi {R_{i,s}^{(m)}}^2 = \eta/M$ for $m = 1, \ldots, M$, that is, all rings have the same area while their total area is equal to η. As η is independent from $R_{o,s}^{(m)}$, if $R_{o,s}^{(m)}$ increases, $R_{i,s}^{(m)}$ grows as well such that η/M remains unchanged. Under this condition, $P_{\text{av}}(\phi)$ can be approximated for a large $R_{o,s}^{(1)}$ as shown by (45) at the bottom of the page. Using (28) in (45), it follows that

$$P_{\text{av}}(\phi) \approx \frac{1}{K} + \left(1 - \frac{1}{K}\right) \left| \frac{\sqrt{2}}{M} \sum_{m=1}^{M} \frac{\cos\left(R_{o,s}^{(m)}\beta(\phi) - \frac{\pi}{4}\right)}{\sqrt{\pi R_{o,s}^{(m)}\beta(\phi)}} \right|^2 \tag{46}$$

for $R_{1,o}\beta(\phi) \gg 1/4$. The above approximation shows that the contributions of all rings to $P_{\text{av}}(\phi)$ are simply summed up inside the absolute value at the right-hand side of (46). This fact facilitates a simple approach to determine $R_{o,s}^{(m)}$, $m = 1, \ldots, M$. Assume that it is required to have a null positioned at ϕ^*. Selecting

$$R_{o,s}^{(m)} = \frac{\lambda\left(m - \frac{1}{4}\right)}{4\sin\left(\frac{\phi^*}{2}\right)}, \quad m = 1, \ldots, M \tag{47}$$

all the cosine functions at the right-hand side of (46) are equal to zero at $\phi = \phi^*$, while each of these functions is maximized at a different set of points

$$\phi_{(p),l}^{(m)} \approx \arcsin\left(\frac{\lambda\left(l + \frac{1}{4}\right)}{4R_{o,s}^{(m)}}\right) \tag{48}$$

for $m = 1, \ldots, M$. This results in generating an average beampattern null at ϕ^* while substantially reducing the sidelobe peaks. Note also that, as all rings reinforce the null at ϕ^*, one may conjecture that the null width around ϕ^* increases as the number of rings grows. Numerical results in Section VI verify this conjecture.

It should be mentioned that, if multiple narrow rings are used, the inter-ring connectivity is maintained when $R_{o,s}^{(m+1)} - R_{o,s}^{(m)} < R_f$ for $m = 1, \ldots, M-1$. However, if the latter inequality does not hold for an m, some of the nodes located between the rings m and $m+1$ may be kept in the active mode and used to establish the connection between those rings. Alternative means to maintain the inter-cluster connectivity [21], [22] may also be adopted to preserve the connection between the rings.

V. Transmission of a Noisy Signal From the DBF Nodes

In this section, we study the case where the DBF nodes have only access to noisy versions of the signal. Such a scenario may occur if, for instance, the DBF nodes fail to reach a consensus or when they receive noisy replicas of the signal that is broadcasted from a source. In such cases, the signal transmitted from the kth node in the nth transmission slot is $s_k(n) = w_k^*(u(n) + v_k(n))$ where $v_k(n)$ is a zero-mean contaminating noise at node k. Let $\mathbf{v}(n) \triangleq [v_1(n) \ \ldots \ v_K(n)]^T$. We do not rule out noises' possible correlations and assume that $\mathbf{\Sigma} = \text{E}\{\mathbf{v}(n)\mathbf{v}(n)^H\}$ is not a diagonal matrix in general. Then, the total transmit power from the DBF nodes is

$$\Upsilon_{\text{ns}} = \mathbf{w}^H(\mathbf{I} + \mathbf{\Delta})\mathbf{w} \tag{49}$$

where $\mathbf{\Delta} \triangleq \text{diag}\left\{\text{E}\left\{|v_1(n)|^2\right\} \ \ldots \ \text{E}\left\{|v_K(n)|^2\right\}\right\} = \text{diag}\left\{[\mathbf{\Sigma}]_{11} \ \ldots \ [\mathbf{\Sigma}]_{KK}\right\}$ with $\text{diag}\{\cdot\}$ denoting a diagonal matrix and $[\cdot]_{i,k}$ standing for the (i,k)th entry of a matrix and $\mathbf{I}$ is the identity matrix. Using similar steps as in those prior to (5), it can be shown that the total received signal at $B_\phi(Q, \phi)$ due to all DBF nodes is

$$\begin{aligned} y_{B_\phi}(n) = {} & GQ^{-\gamma/2}e^{-j(2\pi/\lambda)Q}u(n)\mathbf{w}^H\mathbf{a}_\phi \\ & + GQ^{-\gamma/2}e^{-j(2\pi/\lambda)Q}\mathbf{w}^H(\mathbf{v}(n) \odot \mathbf{a}_\phi) \end{aligned} \tag{50}$$

$$\text{E}\left\{ e^{j\beta(\phi)Z} \right\} = \frac{2}{\sum_{m=1}^{M} {R_{o,s}^{(m)}}^2 - {R_{i,s}^{(m)}}^2} \cdot \left(\sum_{m=1}^{M} \frac{R_{o,s}^{(m)}}{\beta(\phi)} J_1\left(R_{o,s}^{(m)}\beta(\phi)\right) - \frac{R_{i,s}^{(m)}}{\beta(\phi)} J_1\left(R_{i,s}^{(m)}\beta(\phi)\right) \right) \tag{44}$$

$$\begin{aligned} P_{\text{av}}(\phi) &\approx \frac{1}{K} + \left(1 - \frac{1}{K}\right) \lim_{R_{i,s}^{(1)} \to R_{o,s}^{(1)}} \cdots \lim_{R_{i,s}^{(M)} \to R_{o,s}^{(M)}} \left| \frac{2\left(\sum_{m=1}^{M} \frac{R_{o,s}^{(m)}}{\beta(\phi)} J_1\left(R_{o,s}^{(m)}\beta(\phi)\right) - \frac{R_{i,s}^{(m)}}{\beta(\phi)} J_1\left(R_{i,s}^{(m)}\beta(\phi)\right) \right)}{\sum_{m=1}^{M} {R_{o,s}^{(m)}}^2 - {R_{i,s}^{(m)}}^2} \right|^2 \\ &= \frac{1}{K} + \left(1 - \frac{1}{K}\right) \left| \frac{1}{\beta(\phi)M} \sum_{m=1}^{M} \lim_{R_{i,s}^{(m)} \to R_{o,s}^{(m)}} \frac{R_{o,s}^{(m)}\beta(\phi)J_1\left(R_{o,s}^{(m)}\beta(\phi)\right) - R_{i,s}^{(m)}\beta(\phi)J_1\left(R_{i,s}^{(m)}\beta(\phi)\right)}{R_{o,s}^{(m)}(R_{o,s}^{(m)}\beta(\phi) - R_{i,s}^{(m)}\beta(\phi))} \right|^2 \\ &= \frac{1}{K} + \left(1 - \frac{1}{K}\right) \left| \frac{1}{M} \sum_{m=1}^{M} J_0\left(R_{o,s}^{(m)}\beta(\phi)\right) \right|^2 \end{aligned} \tag{45}$$

where $\odot$ is the element-wise product. Let $\mathbf{A}_\phi \triangleq \mathrm{diag}\{\mathbf{a}_\phi\} = \mathrm{diag}\left\{e^{j(2\pi/\lambda)r_1\cos(\phi-\psi_1)} \ \ldots \ e^{j(2\pi/\lambda)r_K\cos(\phi-\psi_K)}\right\}$. It is straightforward to show from (50) that the SNR at the AP is $\Omega_{\mathrm{ns}} = \varsigma\left|\mathbf{w}^H\mathbf{a}_0\right|^2/(\varsigma\mathbf{w}^H\mathbf{A}_0\boldsymbol{\Sigma}\mathbf{A}_0^H\mathbf{w}+\varrho_0^2)$ where the subscript "ns" differentiates the SNR in the noisy sensor case from its noise-free sensor counterpart. Similar to Section II, our goal is to find the optimal beamforming vector that maximizes Ω_{ns} subject to the total power constraint $\Upsilon_{\mathrm{ns}} \leq 1$. In this case, the optimal $\mathbf{w}$ is

$$\mathbf{w}_{\mathrm{ns}} = \frac{\left(\mathbf{A}_0\boldsymbol{\Sigma}\mathbf{A}_0^H+\frac{\varrho_0^2}{\varsigma}(\mathbf{I}+\boldsymbol{\Delta})\right)^{-1}\mathbf{a}_0}{\left\|(\mathbf{I}+\boldsymbol{\Delta})^{1/2}\left(\mathbf{A}_0\boldsymbol{\Sigma}\mathbf{A}_0^H+\frac{\varrho_0^2}{\varsigma}(\mathbf{I}+\boldsymbol{\Delta})\right)^{-1}\mathbf{a}_0\right\|} = \frac{\mathbf{A}_0\left(\boldsymbol{\Sigma}+\frac{\varrho_0^2}{\varsigma}(\mathbf{I}+\boldsymbol{\Delta})\right)^{-1}\mathbf{1}}{\sqrt{\mathbf{1}^T\left(\boldsymbol{\Sigma}+\frac{\varrho_0^2}{\varsigma}(\mathbf{I}+\boldsymbol{\Delta})\right)^{-1}(\mathbf{I}+\boldsymbol{\Delta})\left(\boldsymbol{\Sigma}+\frac{\varrho_0^2}{\varsigma}(\mathbf{I}+\boldsymbol{\Delta})\right)^{-1}\mathbf{1}}} \tag{51}$$

where $\mathbf{1}$ is a vector with all entries equal to 1. Using (51) in (50) and taking the statistical expectation from the square norm of the resulting expression, it can also be readily shown that the total received power at $B_\phi(Q,\phi)$ from the DBF nodes is given by (52), shown at the bottom of the page, where $\mathbf{M}_1(\phi,\mathbf{r},\boldsymbol{\psi}) \triangleq \mathbf{A}_0^H\mathbf{a}_\phi\mathbf{a}_\phi^H\mathbf{A}_0$ and $\mathbf{M}_2(\phi,\mathbf{r},\boldsymbol{\psi}) \triangleq \mathbf{A}_0^H\mathbf{A}_\phi\boldsymbol{\Sigma}\mathbf{A}_\phi^H\mathbf{A}_0$. From the definition of $\mathbf{A}_\phi$ we have

$$\begin{aligned}[\mathbf{M}_1(\phi,\mathbf{r},\boldsymbol{\psi})]_{i,k} &= e^{j(2\pi/\lambda)r_i(\cos(\phi-\psi_i)-\cos(\psi_i))}\cdot e^{-j(2\pi/\lambda)r_k(\cos(\phi-\psi_k)-\cos(\psi_k))}\\ &= e^{j\beta(\phi)z_i}\cdot e^{-j\beta(\phi)z_k} \qquad (53)\\ [\mathbf{M}_2(\phi,\mathbf{r},\boldsymbol{\psi})]_{i,k} &= [\boldsymbol{\Sigma}]_{i,k}e^{j(2\pi/\lambda)r_i(\cos(\phi-\psi_i)-\cos(\psi_i))}\cdot e^{-j(2\pi/\lambda)r_k(\cos(\phi-\psi_k)-\cos(\psi_k))}\\ &= [\boldsymbol{\Sigma}]_{i,k}e^{j\beta(\phi)z_i}\cdot e^{-j\beta(\phi)z_k}. \qquad (54)\end{aligned}$$

In view of (53) and (54) and following the same treatment as in the noise-free sensor case presented in Section II-B, the total received power $\chi_{\mathrm{ns}}(\phi,\mathbf{r},\boldsymbol{\psi})$ can be equivalently represented as (55), shown at the bottom of the page, where $\check{\mathbf{M}}_1(\phi,\mathbf{z})$ and $\check{\mathbf{M}}_2(\phi,\mathbf{z})$ are two matrices whose (i,k)th entries are given by the right-hand sides of (53) and (54), respectively. Similar to the noise-free sensor case, the far-field beampattern $P_{\mathrm{ns}}(\phi,\mathbf{z}) \triangleq \check{\chi}_{\mathrm{ns}}(\phi,\mathbf{z})/\varsigma K$ is an important characteristic of the beamformer as it determines the spatial distribution of the received power from the DBF nodes, and, in particular, the level of interference induced by the WSN cluster on any possible unintended receiver at any arbitrary direction $\phi \neq 0$. The following theorem explores the simple relation between the average beampattern in the noisy sensor case and its noise-free sensor counterpart $P_{\mathrm{av}}(\phi)$.

Theorem 4: Let $P_{\mathrm{ns,av}}(\phi) \triangleq \mathrm{E}_{\mathbb{Z}}\{P_{\mathrm{ns}}(\phi,\mathbb{Z})\}$. We have

$$P_{\mathrm{ns,av}}(\phi) = c_1P_{\mathrm{av}}(\phi)+c_2 \tag{56}$$

where $P_{\mathrm{av}}(\phi)$ is given by (13) when the DBF nodes are selected from a single ring and by (43) and (44) when they are selected from multiple concentric rings and c_1 and c_2 are two constants that do not depend on ϕ and are given by (57) and (58), shown at the bottom of the page. If noises at sensors are uncorrelated and have equal power, that is, $\boldsymbol{\Sigma} = \varrho^2\mathbf{I}$, then (56) simplifies to

$$P_{\mathrm{ns,av}}(\phi) = \frac{1}{1+\varrho^2}P_{\mathrm{av}}(\phi)+\frac{\varrho^2}{K\cdot(1+\varrho^2)}. \tag{59}$$

Proof: See Appendix E.

Note that (59) is in the same spirit as [3, Eq. (16)] that offers an average beampattern expression for an ad-hoc WSN with i.i.d. sensor noises and a different power constraint than the total power constraint used in our work.

Equation (56) shows that $P_{\mathrm{ns,av}}(\phi)$, the average beampattern in the noisy sensor case, is only a scaled and a biased version of $P_{\mathrm{av}}(\phi)$ and, further, the scaling factor and the bias are *not* functions of ϕ and depend only on $\boldsymbol{\Sigma}$. Therefore, $P_{\mathrm{ns,av}}(\phi)$ and

$$\chi_{\mathrm{ns}}(\phi,\mathbf{r},\boldsymbol{\psi}) = \varsigma\cdot\frac{\mathbf{1}^T\left(\boldsymbol{\Sigma}+\frac{\varrho_0^2}{\varsigma}(\mathbf{I}+\boldsymbol{\Delta})\right)^{-1}(\mathbf{M}_1(\phi,\mathbf{r},\boldsymbol{\psi})+\mathbf{M}_2(\phi,\mathbf{r},\boldsymbol{\psi}))\left(\boldsymbol{\Sigma}+\frac{\varrho_0^2}{\varsigma}(\mathbf{I}+\boldsymbol{\Delta})\right)^{-1}\mathbf{1}}{\mathbf{1}^T\left(\boldsymbol{\Sigma}+\frac{\varrho_0^2}{\varsigma}(\mathbf{I}+\boldsymbol{\Delta})\right)^{-1}(\mathbf{I}+\boldsymbol{\Delta})\left(\boldsymbol{\Sigma}+\frac{\varrho_0^2}{\varsigma}(\mathbf{I}+\boldsymbol{\Delta})\right)^{-1}\mathbf{1}} \tag{52}$$

$$\check{\chi}_{\mathrm{ns}}(\phi,\mathbf{z}) = \varsigma\cdot\frac{\mathbf{1}^T\left(\boldsymbol{\Sigma}+\frac{\varrho_0^2}{\varsigma}(\mathbf{I}+\boldsymbol{\Delta})\right)^{-1}(\check{\mathbf{M}}_1(\phi,\mathbf{z})+\check{\mathbf{M}}_2(\phi,\mathbf{z}))\left(\boldsymbol{\Sigma}+\frac{\varrho_0^2}{\varsigma}(\mathbf{I}+\boldsymbol{\Delta})\right)^{-1}\mathbf{1}}{\mathbf{1}^T\left(\boldsymbol{\Sigma}+\frac{\varrho_0^2}{\varsigma}(\mathbf{I}+\boldsymbol{\Delta})\right)^{-1}(\mathbf{I}+\boldsymbol{\Delta})\left(\boldsymbol{\Sigma}+\frac{\varrho_0^2}{\varsigma}(\mathbf{I}+\boldsymbol{\Delta})\right)^{-1}\mathbf{1}} \tag{55}$$

$$c_1 = \frac{\mathbf{1}^T\left(\boldsymbol{\Sigma}+\frac{\varrho_0^2}{\varsigma}(\mathbf{I}+\boldsymbol{\Delta})\right)^{-1}(\mathbf{1}\mathbf{1}^T+\boldsymbol{\Sigma}-\mathbf{I}-\boldsymbol{\Delta})\left(\boldsymbol{\Sigma}+\frac{\varrho_0^2}{\varsigma}(\mathbf{I}+\boldsymbol{\Delta})\right)^{-1}\mathbf{1}}{(K-1)\cdot\mathbf{1}^T\left(\boldsymbol{\Sigma}+\frac{\varrho_0^2}{\varsigma}(\mathbf{I}+\boldsymbol{\Delta})\right)^{-1}(\mathbf{I}+\boldsymbol{\Delta})\left(\boldsymbol{\Sigma}+\frac{\varrho_0^2}{\varsigma}(\mathbf{I}+\boldsymbol{\Delta})\right)^{-1}\mathbf{1}} \tag{57}$$

$$c_2 = \frac{\mathbf{1}^T\left(\boldsymbol{\Sigma}+\frac{\varrho_0^2}{\varsigma}(\mathbf{I}+\boldsymbol{\Delta})\right)^{-1}(K\mathbf{I}+K\boldsymbol{\Delta}-\mathbf{1}\mathbf{1}^T-\boldsymbol{\Sigma})\left(\boldsymbol{\Sigma}+\frac{\varrho_0^2}{\varsigma}(\mathbf{I}+\boldsymbol{\Delta})\right)^{-1}\mathbf{1}}{K(K-1)\cdot\mathbf{1}^T\left(\boldsymbol{\Sigma}+\frac{\varrho_0^2}{\varsigma}(\mathbf{I}+\boldsymbol{\Delta})\right)^{-1}(\mathbf{I}+\boldsymbol{\Delta})\left(\boldsymbol{\Sigma}+\frac{\varrho_0^2}{\varsigma}(\mathbf{I}+\boldsymbol{\Delta})\right)^{-1}\mathbf{1}} \tag{58}$$

$P_{\rm av}(\phi)$ share exactly the same set of null and peak positions, respectively, at $\phi_{(n),l}$ and $\phi_{(p),l}$ while we have $P_{\rm ns,av}(\phi_{(n),l}) = c_1 P_{\rm av}(\phi_{(n),l}) + c_2$ and $P_{\rm ns,av}(\phi_{(p),l}) = c_1 P_{\rm av}(\phi_{(p),l}) + c_2$. Similar to the noise-free sensor scenario discussed in Section III-A, it follows from (56) that when selecting the active nodes from a close vicinity of the perimeter of $D(O, R_{o,s})$, the mainlobe of $P_{\rm ns,av}(\phi)$ can also be shrunk by up to 37% compared to the case that the nodes are randomly selected from the whole $D(O, R_{o,s})$. Following a similar discussion as in Sections III-B and III-C, it also holds that both the network energy waste and the node isolation probability are substantially reduced in the former case. The approximate expressions of $P_{\rm av}(\phi)$ derived in (27) and (29) for a single narrow ring and in (45) and (46) for multiple concentric narrow rings can also be used in (56) to obtain the counterpart approximations of $P_{\rm ns,av}(\phi)$. Moreover, when it is required to position a null in a particular direction, it is possible to do so by selecting the rings outer radii from (47). In light of (56), the results regarding the average directivity of the beampattern presented in Section III-E and the statistical behavior of the beampattern obtained in Section III-F can also be straightforwardly generalized to the noisy sensor case.

VI. Simulations

Numerical simulations are used to validate the analytical results derived in Sections III and IV. In all examples, $\lambda = 10$ m is selected. Fig. 2 shows $P_{\rm av}(\phi)$ versus ϕ for the case that $K = 20$ nodes are randomly selected from $S(O, \alpha R_{o,s}, R_{o,s})$ with $R_{o,s} = 100\lambda$ and four different values of $\alpha = 0,\ 0.3,\ 0.7,\ 0.998$. Note that, $\alpha = 0.998$ corresponds to the case that the nodes are selected from $S(O, 998\ \mathrm{m}, 1000\ \mathrm{m})$ and, assuming that $\rho = 0.1\ \mathrm{m}^{-2}$, the expected number of nodes located on the latter ring is $\zeta = \rho A_S \approx 1225$. Moreover, the inner and outer radii of $S(O, 998\ \mathrm{m}, 1000\ \mathrm{m})$ satisfy (22). Assuming that $R_f = \lambda$, we have obtained $R_{o,d} \approx 177.25$ m from (26) and, for the sake of comparison, we have also plotted $P_{\rm av}(\phi)$ in the case that the nodes are selected from $D(O, R_{o,d})$. Recalling our discussion in Section III-C, if the numbers of active nodes in both $S(O, 998\ \mathrm{m}, 1000\ \mathrm{m})$ and $D(O, R_{o,d})$ are equal, then the probability of node isolation in both cases is almost the same. As can be observed from Fig. 2, increasing α results in decreasing $\phi_{(n),1}$. Moreover, $\phi_{(n),1}$ corresponding to $\alpha = 0$ and $\alpha = 0.998$ are in fact very close to the analytical values obtained in (20) and (21), respectively. Finally, all curves have only one null in $\left[2\arcsin\left((4\pi R_{o,s})^{-1}\lambda\nu_0\right),\ 2\arcsin\left((4\pi R_{o,s})^{-1}\lambda\nu_1\right)\right]$. The above observations verify the results of Theorem 1. Fig. 2 also shows that the peak values of $P_{\rm av}(\phi)$ increase with an increasing α. However, even when $\alpha = 0.998$, the average beampattern still enjoys much higher directivity than its disc-based counterpart wherein the nodes are selected from $D(O, R_{o,d})$. The first row of Table I shows $\tilde{D}_{\rm av}/K$ with $K = 20$ for the four considered values of α as well as for the case that the nodes are selected from $D(O, R_{o,d})$. As can be observed from Table I, when the nodes are selected from $S(O, \alpha \cdot 1000\ \mathrm{m}, 1000\ \mathrm{m})$, increasing α results in a small reduction in $\tilde{D}_{\rm av}/K$. At the same time, $\tilde{D}_{\rm av}/K$ for $\alpha = 0.998$ is substantially larger than $\tilde{D}_{\rm av}/K$ when the nodes are selected from $D(O, R_{o,d})$.

Fig. 3 shows the same curves as in Fig. 2 for $K = 200$. While all curves have deeper nulls in Fig. 3, most of the observations made above from Fig. 2 also hold in this example. The second row of Table I gives $\tilde{D}_{\rm av}/K$ for all cases considered in Fig. 3.

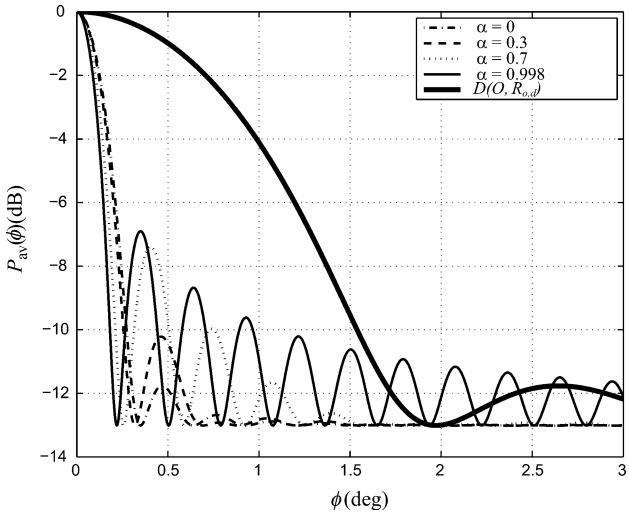

Fig. 2. $P_{\rm av}(\phi)$ (dB) versus ϕ (deg) for $K = 20$.

TABLE I
$\tilde{D}_{\rm av}/K$ FOR $K = 20$ AND $K = 200$ AND DIFFERENT α

	$\alpha = 0$	$\alpha = 0.3$	$\alpha = 0.7$	$\alpha = 0.998$	$D(O, 177.25\ m)$
$K = 20$	0.98	0.98	0.98	0.97	0.91
$K = 200$	0.85	0.85	0.85	0.76	0.51

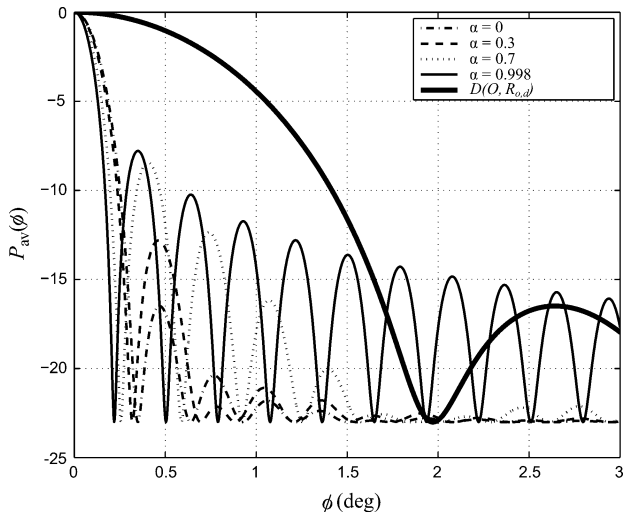

Fig. 3. $P_{\rm av}(\phi)$ (dB) versus ϕ (deg) for $K = 200$.

Again, the table shows that $\tilde{D}_{\rm av}/K$ for $\alpha = 0.998$ is considerably higher than $\tilde{D}_{\rm av}/K$ when the nodes are selected from $D(O, R_{o,d})$.

The accuracy of (29) and (30) to model the behavior of $P_{\rm av}(\phi)$ for a large α is examined in Fig. 4. First, assuming the target $\phi_{(n),1} = 2$ (deg), $R_{o,s}$ is derived from (30). Then, the so-obtained $R_{o,s}$ and $K = 20$ are used to plot the approximate $P_{\rm av}(\phi)$ for $\alpha \longrightarrow 1^-$ from (29). The same K and $R_{o,s}$ are also used to plot the limiting $P_{\rm av}(\phi)$ for $\alpha \longrightarrow 1^-$ from (27) as well as $P_{\rm av}(\phi)$ curves for $\alpha = 0.9$, $\alpha = 0.95$, and $\alpha = 0.998$ from (13). It can be observed from Fig. 4 that $P_{\rm av}(\phi)$ curves obtained from (29) and (27) are almost indistinguishable throughout the whole range of examined ϕ. This verifies the accuracy of (27)

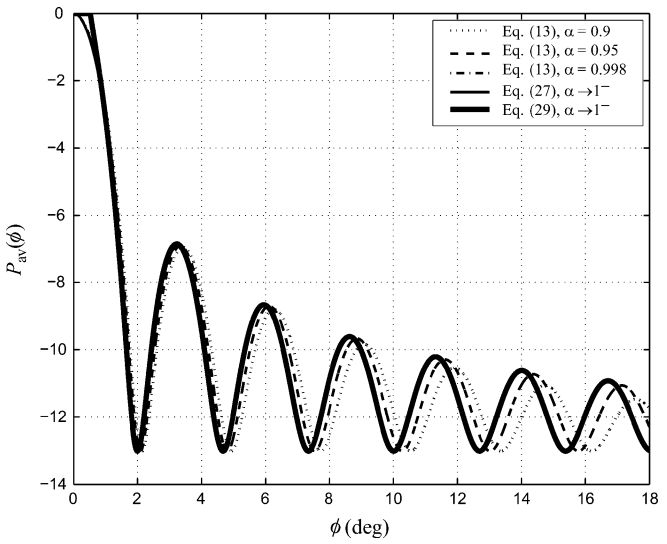

Fig. 4. $P_{\rm av}(\phi)$ (dB) versus ϕ (deg) for $\alpha \approx 1$.

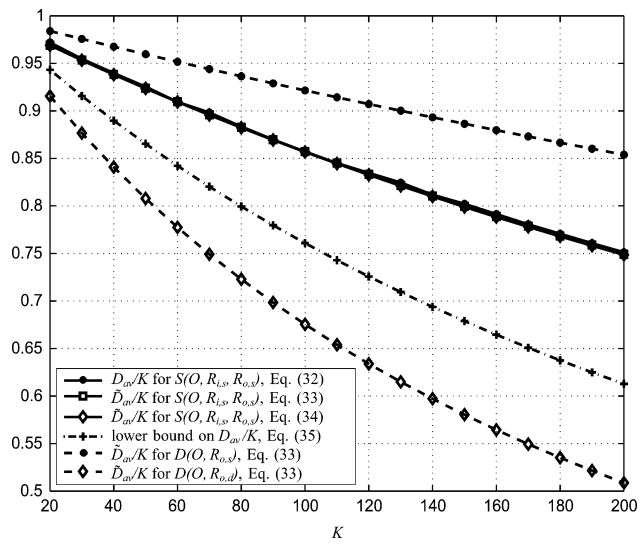

Fig. 5. Normalized average directivity and its lower bounds versus K.

in predicting the behavior of the average beampattern when α approaches to one. Note from Fig. 4 that the curves drawn from (27) and (29) closely follow those obtained from (13) especially for a small ϕ. For larger values of ϕ, the smaller the α, the more the deviation of its corresponding $P_{\rm av}(\phi)$ curve from the limiting curves (27) and (29). Finally, as can be observed from the figure, $\phi_{(n),1}$ is very close to the target value of 2 (deg) in all curves. This confirms the reliability of (30) in estimating the first null of the average beampattern when α is close to 1.

In Figs. 5–7, $\rho = 0.1\ \mathrm{m}^{-2}$ and $\zeta = 300$ is selected. Moreover, for any given $R_{o,s}$, $R_{i,s} = \sqrt{R_{o,s}^2 - \zeta/(\pi\rho)}$ is chosen to guarantee that the expected number of nodes on the ring is in fact equal to ζ.

In Fig. 5, $R_{o,s} = 100\lambda$ is selected. This figure shows the normalized versions of $\tilde{D}_{\rm av}$ in (33) as well as the average directivity $D_{\rm av}$ in (32) where the nodes are selected from $S(O, R_{i,s}, R_{o,s})$ and the average is taken over 1000 independent realizations of the node locations. Fig. 5 also displays the normalized version of $\tilde{D}_{\rm av}$ curve in (34) derived for the case that $R_{i,s} \longrightarrow R_{o,s}$ along with the curve corresponding to the lower-bound obtained in (35). Finally, for the sake of comparison, we have also shown the normalized versions of $\tilde{D}_{\rm av}$ in (33) for the scenarios wherein the nodes are selected from $D(O, R_{o,s})$ and $D(O, R_{o,d})$ where $R_{o,d}$ is obtained from (26) with $R_f = \lambda$. As can be observed from Fig. 5, the normalized average directivity curve is very closely followed by the normalized versions of $\tilde{D}_{\rm av}$ curves obtained from (33) and (34). This verifies that (33) is in fact a tight lower bound on the average directivity. Moreover, it shows that, for the selected values of ρ, ζ, and $R_{o,s}$, $\tilde{D}_{\rm av}$ expression in (34) accurately predicts the beampattern directivity. Fig. 5 also shows that although the simple lower-bound obtained in (35) is correct, it is quite conservative especially for larger values of K. It is also important to observe that the directivity when the nodes are selected from $S(O, R_{i,s}, R_{o,s})$ is substantially larger than the directivity when the nodes are chosen from $D(O, R_{o,d})$ while being less than the directivity when the nodes are chosen from $D(O, R_{o,s})$. However, recalling our discussion in Section III-C, it should be taken into consideration that when the nodes are selected from $D(O, R_{o,s})$, the probability of node isolation is much higher than the case that the nodes are selected from $S(O, R_{i,s}, R_{o,s})$ or $D(O, R_{o,d})$.

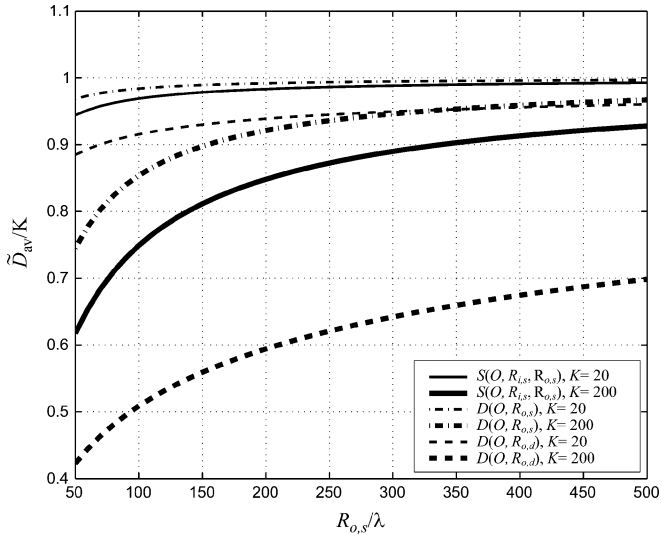

Fig. 6. $\bar{D}_{\rm av}/K$ versus $R_{o,s}/\lambda$ for $K = 20$ and $K = 200$ and corresponding to the cases that the nodes are selected from $S(O, R_{i,s}, R_{o,s})$, $D(O, R_{o,s})$, and $D(O, R_{o,d})$.

Fig. 6 displays $\tilde{D}_{\rm av}/K$ versus $R_{o,s}/\lambda$ for $K = 20$ and $K = 200$ and three different cases that the nodes are selected from $S(O, R_{i,s}, R_{o,s})$, $D(O, R_{o,s})$, and $D(O, R_{o,d})$ where $R_{o,d}$ is obtained from (26) using $R_f = \lambda$. Fig. 6 shows that selecting the nodes from $S(O, R_{i,s}, R_{o,s})$ and $D(O, R_{o,s})$ results in approximately equal $\tilde{D}_{\rm av}/K$ throughout the whole range of examined $R_{o,s}$. This substantiates the advantage of selecting the nodes from $S(O, R_{i,s}, R_{o,s})$ that is associated with a much more favorable network connectivity condition. It can also be observed from Fig. 6 that when the nodes are selected from $D(O, R_{o,d})$ which has a network connectivity condition similar to $S(O, R_{i,s}, R_{o,s})$, the directivity significantly degrades. This further corroborates our discussion at the end of Section III-C.

Fig. 7 shows $\tilde{D}_{\rm av}/K$ versus $R_{o,s}/\lambda$ corresponding to the case that $K = 200$ nodes are selected from $S(O, R_{i,s}, R_{o,s})$. This

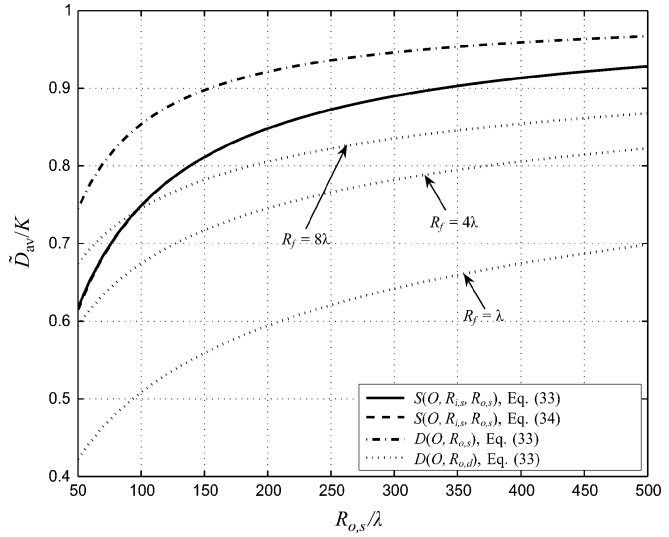

Fig. 7. $\bar{D}_{\rm av}/K$ versus $R_{o,s}/\lambda$ for the cases that the nodes are chosen from $S(O, R_{i,s}, R_{o,s})$, $D(O, R_{o,s})$, and $D(O, R_{o,d})$ with $R_{o,d}$ corresponding to $R_f = \lambda$, $R_f = 4\lambda$, and $R_f = 8\lambda$.

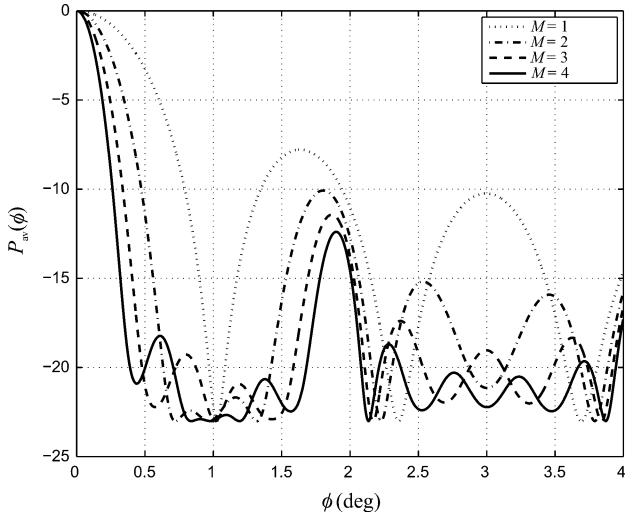

Fig. 8. $P_{\rm av}(\phi)$ versus ϕ (deg) for $K = 200$ and $M = 1,\ 2,\ 3$, and 4.

curve is compared with the limiting $\tilde{D}_{\rm av}/K$ curve derived in (34) as well as $\tilde{D}_{\rm av}/K$ curves corresponding to the cases that the nodes are selected from $D(O, R_{o,d})$ with three different $R_{o,d}$ values obtained from (26) for $R_f = \lambda$, $R_f = 4\lambda$, and $R_f = 8\lambda$. This figure also draws $\tilde{D}_{\rm av}/K$ curve for the scenario in which the nodes are selected from $D(O, R_{o,s})$. Note from Fig. 7 that the actual and the limiting $\tilde{D}_{\rm av}/K$ curves are almost indistinguishable. This further verifies the accuracy of the asymptotic $\tilde{D}_{\rm av}/K$ expression in (34) in approximating the actual value of $\tilde{D}_{\rm av}/K$ when $S(O, R_{i,s}, R_{o,s})$ is a large narrow ring. It can also be observed from Fig. 7 that, even for an R_f as large as 8λ, the directivity when the nodes are selected from $S(O, R_{i,s}, R_{o,s})$ is higher than the case when the nodes are chosen from $D(O, R_{o,d} = \sqrt{\pi R_f R_{o,s}})$.

Fig. 8 demonstrates the effect of using multiple concentric rings on $P_{\rm av}(\phi)$. Four cases of $M = 1,\ 2,\ 3$, and 4 are considered. In each case, the desired first null of the average beampattern is set to $\phi_{(n),1} = \phi^* = 1$ (deg) and (47) is used to obtain $R_{o,s}^{(m)}$ for $m = 1, \ldots, M$. Then, $\rho = 0.1\ m^{-2}$ and $\zeta = 300$ are used to derive η, the aggregate area of the M rings. Finally, assuming that all M rings have the same area, $R_{i,s}^{(m)}$ are achieved for $m = 1, \ldots, M$. As can be observed from Fig. 8, all four curves have a null at $\phi^* = 1$ (deg). Moreover, increasing M, not only the sidelobe peak levels substantially decrease, but also the null width around $\phi^* = 1$ increases. This validates our discussion in Section IV.

VII. Conclusions

A transmit beamforming technique was studied in wireless sensor networks with uniformly distributed nodes and the effects of node selection on the average beampattern, the energy efficiency, and the network connectivity were investigated. The average beampattern expression was obtained for the general case that the beamforming nodes are located on a ring with arbitrary inner and outer radii and it was shown that increasing the inner radius, or, equivalently, selecting the nodes from a vicinity of the ring's outer boundary, not only results in narrowing the average beampattern mainlobe but also in a more energy efficiency and a less node isolation probability. In the case that the beamforming nodes are located on a large narrow ring, a simple approximate expression for the average beampattern was obtained and a tight lower bound on the average beampattern directivity was derived. It was shown that the lower bound approaches to one with a minimum rate similar to that of the technique proposed in [1]. Statistical properties of the beampattern were analyzed and an approximate expression for the complementary cumulative distribution function of the beampattern was derived. The techniques was then generalized to the case that the nodes are chosen from multiple concentric rings and it was shown how the rings' radii can be properly selected to substantially reduce the sidelobe peak levels. A SNR-optimal beamforming vector was also obtained in the case when the DBF nodes only have access to noisy versions of the signal and a simple relation was established between the beampattern expressions in the noise-free and noisy sensor cases.

Appendix A
Preliminary Results

Theorem 5: Consider M concentric rings[4] $S_m(O, R_{i,s}^{(m)}, R_{o,s}^{(m)})$ with $R_{o,s}^{(m)} < R_{i,s}^{(m+1)}$, $m = 1, \ldots, M-1$ and a random point $T(R, \Psi)$ where R and Ψ respectively denote the radial and the angular coordinates of T in the polar coordinate system with origin O and an arbitrary x axis. Assume that T is uniformly distributed on the region $\mathcal{S}_M = \cup_{m=1}^{M} S_m$ (shown by hashes in Fig. 9), that is,

$$f_R(r) = \begin{cases} 2rA_{\mathcal{S}_M}^{-1} & r \in \cup_{m=1}^{M}[R_{i,s}^{(m)}, R_{o,s}^{(m)}] \\ 0 & \text{elsewhere} \end{cases}$$
$$f_\Psi(\psi) = \frac{1}{2\pi} \quad \psi \in [0, 2\pi) \tag{60}$$

where $A_{\mathcal{S}_M} = \pi \sum_{m=1}^{M} {R_{o,s}^{(m)}}^2 - {R_{i,s}^{(m)}}^2$ is the area of $\mathcal{S}_M$. Let $\xi_{o,m}(z) \triangleq R_{o,s}^{(m)}\sqrt{1 - \left(z/R_{o,s}^{(m)}\right)^2}$ and $\xi_{i,m}(z) \triangleq R_{i,s}^{(m)}\sqrt{1 - \left(z/R_{i,s}^{(m)}\right)^2}$. Then, the PDF of $Z \triangleq R\sin(\Psi)$ is given by (61), shown at the bottom of

[4]Equation (9) is a special case of Theorem 5 for $M = 1$.

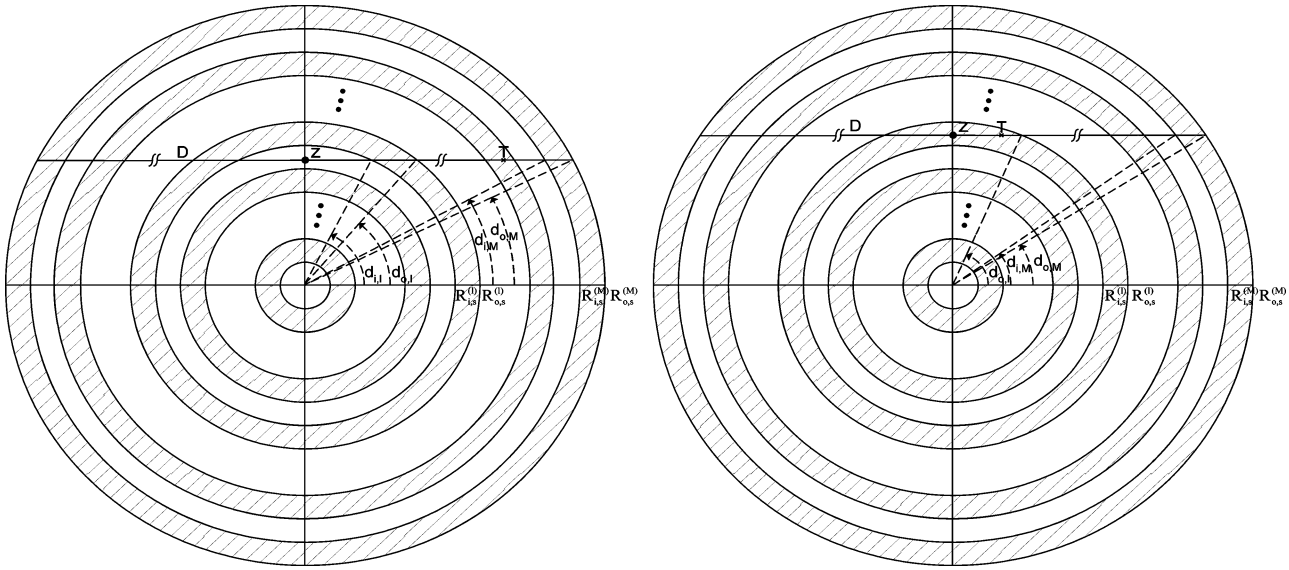

Fig. 9. M concentric rings with $R_{o,s}^{(l-1)} \leq z < R_{i,s}^{(l)}$ (left subfigure) and $R_{i,s}^{(l)} \leq z < R_{o,s}^{(l)}$ (right subfigure).

the page, where $R_{o,0} \triangleq 0$ and the superscript of $f_Z^{(M)}(z)$ is used to emphasize the number of rings.

Proof: It is direct to show that $f_Z^{(M)}(z) = f_Z^{(M)}(-z)$. Therefore, without any loss of generality, we prove the theorem for $z \geq 0$. For any $z \geq 0$, there is an $l = 1, \ldots, M$ such that $R_{o,l-1} \leq z < R_{o,l}$. Using the fact that T is uniformly distributed on $\mathcal{S}_M$, we have

$$f_Z^{(M)}(z) = -\frac{d}{dz} P(Z > z) = -\frac{d}{dz} \left(\frac{\sum_{m=l}^{M} A_{S_{m,D}}}{A_{\mathcal{S}_M}} \right) \quad (62)$$

where $A_{S_{m,D}}$ is the area of a part of S_m that is above the line D (see Fig. 9). Let us first assume that $R_{o,l-1} \leq z < R_{i,s}^{(l)}$. From the left subfigure of Fig. 9 it can be readily shown that

$$A_{S_{m,D}} = \frac{1}{2} R_{o,s}^{(m)^2} (\pi - 2d_{o,m}) - \frac{1}{2} R_{i,s}^{(m)^2} (\pi - 2d_{i,m}) - z(R_{o,s}^{(m)} \cos d_{o,m} - R_{i,s}^{(m)} \cos d_{i,m}) \quad (63)$$

for $m = l, \ldots, M$. Note that $d_{o,m} = \arcsin(z/R_{o,s}^{(m)})$ and $d_{i,m} = \arcsin(z/R_{i,s}^{(m)})$. Using the latter equalities in (63) and substituting the resulting expression in (62), the first equation of (61) follows. For the case when $R_{i,s}^{(l)} \leq z < R_{o,l}$, it can be observed from the right subfigure of Fig. 9 that

$$A_{S_{l,D}} = \frac{1}{2} R_{o,l}^2 (\pi - 2d_{o,l}) - z R_{o,l} \cos d_{o,l}, \quad (64)$$

while $A_{S_{m,D}}$ is given by (63) for $m = l+1, \ldots, M$. Using (64) and (63) in (62), the second equation of (61) follows.

Proof of (12) and (44): We prove (44) for a general M. Equation (12) is treated as a special case of (44) for $M = 1$. The following lemma is essential for the main proof presented in Theorem 6.

Lemma 1: For any arbitrary scalars t and β we have

$$\int_{-t}^{t} t e^{j\beta z} \sqrt{1 - \left(\frac{z}{t}\right)^2} dz = \frac{t\pi}{\beta} J_1(t\beta). \quad (65)$$

Proof: Introducing $\cos\theta \triangleq z/t$, it is direct to show that

$$\int_{-t}^{t} t e^{j\beta z} \sqrt{1 - \left(\frac{z}{t}\right)^2} dz = \int_0^{\pi} t^2 \sin^2\theta e^{jt\beta\cos\theta} d\theta = \frac{t}{j\beta} \int_0^{\pi} e^{jt\beta\cos\theta} \cos\theta d\theta \quad (66)$$

where the second equation is obtained using integration by parts. Taking into account the fact that $J_n(x) = 1/j^n\pi \int_0^{\pi} e^{jx\cos\theta} \cos(n\theta) d\theta$, (65) follows from (66). This completes the proof.

Theorem 6: Consider Z as described in Theorem 5. We have

$$\mathrm{E}\left\{e^{j\beta z}\right\} = \frac{2}{\sum_{m=1}^{M} R_{o,s}^{(m)^2} - R_{i,s}^{(m)^2}} \cdot \left(\sum_{m=1}^{M} \frac{R_{o,s}^{(m)}}{\beta} J_1\left(R_{o,s}^{(m)}\beta\right) - \frac{R_{i,s}^{(m)}}{\beta} J_1\left(R_{i,s}^{(m)}\beta\right) \right) \quad (67)$$

where β is an arbitrary scalar.

$$f_Z^{(M)}(z) = \begin{cases} 2A_{\mathcal{S}_M}^{-1} \sum_{m=l}^{M} \xi_{o,m}(z) - \xi_{i,m}(z) & R_{o,l-1} \leq |z| < R_{i,s}^{(l)} \\ 2A_{\mathcal{S}_M}^{-1} \left(\xi_{o,l} + \sum_{m=l+1 \leq M}^{M} \xi_{o,m}(z) - \xi_{i,m}(z) \right) & R_{i,s}^{(l)} \leq |z| < R_{o,l} \end{cases} \quad l = 1, \ldots, M \quad (61)$$

$$\begin{aligned}\mathrm{E}\left\{e^{j\beta z}\right\} &= \frac{2}{\pi\left(R_{o,s}^{(1)^2}-R_{i,s}^{(1)^2}\right)}\int_{-R_{o,s}^{(1)}}^{-R_{i,s}^{(1)}}\xi_{o,1}(z)e^{j\beta z}dz+\int_{-R_{i,s}^{(1)}}^{R_{i,s}^{(1)}}\xi_{o,1}(z)-\xi_{i,1}(z)e^{j\beta z}dz+\int_{R_{i,s}^{(1)}}^{R_{o,s}^{(1)}}\xi_{o,1}(z)e^{j\beta z}dz\\ &= \frac{2}{\pi\left(R_{o,s}^{(1)^2}-R_{i,s}^{(1)^2}\right)}\int_{-R_{o,s}^{(1)}}^{R_{o,s}^{(1)}}\xi_{o,1}(z)e^{j\beta z}dz-\int_{-R_{i,s}^{(1)}}^{R_{i,s}^{(1)}}\xi_{i,1}(z)e^{j\beta z}dz\\ &= \frac{2}{R_{o,s}^{(1)^2}-R_{i,s}^{(1)^2}}\left(\frac{R_{o,s}^{(1)}}{\beta}J_1(R_{o,s}^{(1)}\beta)-\frac{R_{i,s}^{(1)}}{\beta}J_1(R_{i,s}^{(1)}\beta)\right)\end{aligned} \tag{69}$$

$$f_Z^{(l+1)}(z)=\begin{cases}2A_{\mathcal{S}_{l+1}}^{-1}\xi_{o,l+1}(z) & R_{i,s}^{(l+1)}\le|z|<R_{o,s}^{(l+1)}\\ 2A_{\mathcal{S}_{l+1}}^{-1}\left(\xi_{o,l+1}(z)-\xi_{i,l+1}(z)\right) & R_{o,s}^{(l)}\le|z|<R_{i,s}^{(l+1)}\\ 2A_{\mathcal{S}_{l+1}}^{-1}\left(\xi_{o,l+1}(z)-\xi_{i,l+1}(z)+0.5A_{\mathcal{S}_l}f_Z^{(l)}(z)\right) & |z|<R_{o,s}^{(l)}\end{cases} \tag{70}$$

$$\begin{aligned}\mathrm{E}\left\{e^{j\beta z}\right\} =& 2A_{\mathcal{S}_{l+1}}^{-1}\left(\int_{-R_{o,s}^{(l+1)}}^{-R_{i,s}^{(l+1)}}e^{j\beta z}\xi_{o,l+1}(z)dz+\int_{-R_{i,s}^{(l+1)}}^{-R_{o,s}^{(l)}}e^{j\beta z}\left(\xi_{o,l+1}(z)-\xi_{i,l+1}(z)\right)dz+0.5A_{\mathcal{S}_l}\int_{-R_{o,s}^{(l)}}^{R_{o,s}^{(l)}}e^{j\beta z}f_Z^{(l)}(z)dz\right.\\ &\left.+\int_{-R_{o,s}^{(l)}}^{R_{o,s}^{(l)}}e^{j\beta z}\left(\xi_{o,l+1}(z)-\xi_{i,l+1}(z)\right)dz+\int_{R_{o,s}^{(l)}}^{R_{i,s}^{(l+1)}}e^{j\beta z}\left(\xi_{o,l+1}(z)-\xi_{i,l+1}(z)\right)dz+\int_{R_{i,s}^{(l+1)}}^{R_{o,s}^{(l+1)}}e^{j\beta z}\xi_{o,l+1}(z)dz\right)\\ =& 2A_{\mathcal{S}_{l+1}}^{-1}\left(\int_{-R_{o,s}^{(l+1)}}^{R_{o,s}^{(l+1)}}e^{j\beta z}\xi_{o,l+1}(z)dz-\int_{-R_{i,s}^{(l+1)}}^{R_{i,s}^{(l+1)}}e^{j\beta z}\xi_{i,l+1}(z)dz+\pi\sum_{m=1}^{l}\frac{R_{o,s}^{(m)}}{\beta}J_1\left(R_{o,s}^{(m)}\beta\right)-\frac{R_{i,s}^{(m)}}{\beta}J_1\left(R_{i,s}^{(m)}\beta\right)\right)\\ =& \frac{2}{\sum_{m=1}^{l+1}R_{o,s}^{(m)^2}-R_{i,s}^{(m)^2}}\left(\sum_{m=1}^{l+1}\frac{R_{o,s}^{(m)}}{\beta}J_1\left(R_{o,s}^{(m)}\beta\right)-\frac{R_{i,s}^{(m)}}{\beta}J_1\left(R_{i,s}^{(m)}\beta\right)\right)\end{aligned} \tag{71}$$

Proof: Proof is by induction over M. According to (61), for $M=1$ we have

$$f_Z^{(M)}(z)=\begin{cases}\frac{2(\xi_{o,1}(z)-\xi_{i,1}(z))}{\pi\left(R_{o,s}^{(1)^2}-R_{i,s}^{(1)^2}\right)} & 0\le|z|<R_{i,s}^{(1)}\\ \frac{2\xi_{o,1}(z)}{\pi\left(R_{o,s}^{(1)^2}-R_{i,s}^{(1)^2}\right)} & R_{i,s}^{(1)}\le|z|<R_{o,s}^{(1)}.\end{cases} \tag{68}$$

From (68), we obtain (69), shown at the top of the page. Note that the last equality of (69) follows from (65). This proves (67) for $M=1$. It remains to show that if (67) holds for $M=l$, it also holds for $M=l+1$. To show this, it is useful to express $f_Z^{(l+1)}(z)$ in terms of $f_Z^{(l)}(z)$. This is done in (70), shown at the top of the page. Equation (70) can be used to obtain (71), shown at the top of the page, for $M=l+1$. Note that the second equation of (71) follows from the assumption that (67) holds for $M=l$ and the third equation of (71) is due to (65). Equation (71) shows that (67) holds for $M=l+1$. This completes the proof.

Appendix B
Proof of Theorem 1

First, note that $f(x,0)=2J_1(x)/x$. This directly yields (16). To prove (17), we have

$$\begin{aligned}\lim_{\alpha\longrightarrow 1^-}f(x,\alpha) &= \lim_{\alpha\longrightarrow 1^-}\left(\frac{J_1(x)-\alpha J_1(\alpha x)}{x-\alpha x}\right)\\ &= \frac{1}{x}\cdot\frac{d(xJ_1(x))}{dx}\\ &= J_0(x).\end{aligned} \tag{72}$$

Equation (17) is a direct result of (72). To proceed to the proof of (18), we first need to show that

$$f(x,\alpha)>0,\quad \text{for}\quad x\in(0,\nu_0]\ \text{and}\ \alpha\in(0,1). \tag{73}$$

Let $h_1(x,\xi)\triangleq\xi xJ_1(\xi x)$. We have

$$\begin{aligned}f(x,\alpha) &= \frac{2}{(1+\alpha)x^2}\cdot\frac{h_1(x,1)-h_1(x,\alpha)}{1-\alpha}\\ &= \frac{2}{(1+\alpha)x^2}\cdot\frac{\partial h_1(x,\xi)}{\partial\xi}\mid_{\xi=c_1}\\ &= \frac{2c_1}{(1+\alpha)}\cdot J_0(c_1x)\end{aligned} \tag{74}$$

where $c_1\in(\alpha,1)$ and the second equality in (74) is due to the mean value theorem. Note that as $x\in(0,\nu_0]$ and $c_1\in(\alpha,1)$, we have that $c_1x\in(0,\nu_0)$, and, therefore, $J_0(c_1x)>0$. This establishes (73). An immediate result of (73) is that $x^*(\alpha)>\nu_0$ for $\alpha\in(0,1)$. We also have $f(\nu_1,\alpha)=-2\alpha J_1(\alpha\nu_1)/(\nu_1(1-\alpha^2))<0$ for $\alpha\in(0,1)$. The latter inequality along with (73) show that for any given $\alpha\in(0,1)$, the sign of $f(x,\alpha)$ changes in $x\in(\nu_0,\nu_1)$. As $f(x,\alpha)$ is continuous, the latter result along with the fact that $x^*(\alpha)>\nu_0$ prove (18).

Now, we need to prove that, $x^*(\alpha)$ is the only root of $f(x,\alpha)$ in (ν_0,ν_1) for any given $\alpha\in(0,1)$. Note that, if $x^*(\alpha)$ and

$\tilde{x}(\alpha)$ are two distinct roots of $f(x,\alpha)$ in (ν_0,ν_1) and, moreover, $\partial f(x,\alpha)/\partial x \mid_{x=x^*(\alpha)} < 0$ and $\partial f(x,\alpha)/\partial x \mid_{x=\tilde{x}(\alpha)} < 0$, then, considering the fact that $f(x,\alpha)$ is continuous, there must be a third distinct root $\hat{x}(\alpha) \in (x^*(\alpha),\tilde{x}(\alpha))$ such that $\partial f(x,\alpha)/\partial x \mid_{x=\hat{x}(\alpha)} \geq 0$. Therefore, to be able to show that $x^*(\alpha)$ is the only root of $f(x,\alpha)$ in (ν_0,ν_1), it is sufficient to prove that

$$\frac{\partial f(x,\alpha)}{\partial x} \mid_{x=\bar{x}} < 0 \tag{75}$$

for any $\bar{x} \in (\nu_0,\nu_1)$ that $f(\bar{x},\alpha)=0$. To prove (75), note that if $\bar{x}$ is a root of $f(\bar{x},\alpha)=0$, then

$$\frac{\partial f(x,\alpha)}{\partial x} \mid_{x=\bar{x}} = \frac{2}{(1-\alpha^2)\bar{x}} \cdot \left(J_0(\bar{x}) - \alpha^2 J_0(\alpha\bar{x})\right) \tag{76}$$

and, hence, we require to show that

$$J_0(\bar{x}) - \alpha^2 J_0(\alpha\bar{x}) < 0. \tag{77}$$

The proof of (77) is by contradiction. Let us assume that

$$J_0(\bar{x}) - \alpha^2 J_0(\alpha\bar{x}) \geq 0. \tag{78}$$

Since $\bar{x} \in (\nu_0,\nu_1)$, we have $J_0(\bar{x}) < 0$. The latter result along with (78) yield $J_0(\alpha\bar{x}) < 0$. This, in turn, implies that $\bar{x} > \nu_0/\alpha$. Let us introduce $h_2(\xi) \triangleq \xi^2 J_0(\xi\bar{x})$. Due to (78), $h_2(1) - h_2(\alpha) \geq 0$, and, hence, there is a $c_2 \in (\alpha,1)$ such that $dh_2(\xi)/d\xi \mid_{\xi=c_2} = 2c_2 J_0(c_2\bar{x}) - c_2^2\bar{x}J_1(c_2\bar{x}) \geq 0$. Form the latter inequality we have that $2J_0(c_2\bar{x}) \geq c_2\bar{x}J_1(c_2\bar{x})$. As $c_2\bar{x} < \nu_1$, the right-hand side of the latter inequality is larger than zero, and, therefore, $c_2\bar{x} < \nu_0$. This, along with the fact that $c_2 > \alpha$, imply that $\bar{x} < \nu_0/\alpha$. The latter inequality contradicts our earlier result that $\bar{x} > \nu_0/\alpha$. This proves the correctness of (75) and, consequently, the uniqueness of the root of $f(x,\alpha)=0$ in (ν_0,ν_1). It remains to prove (19). As $x^*(\alpha)$ is a solution to $f(x,\alpha)=0$,

$$x^*(\alpha)J_1(x^*(\alpha)) - \alpha x^*(\alpha)J_1(\alpha x^*(\alpha)) = 0. \tag{79}$$

From the latter equation, it is direct to show that

$$\frac{dx^*(\alpha)}{d\alpha} = \frac{\alpha x^*(\alpha)J_0(\alpha x^*(\alpha))}{J_0(x^*(\alpha)) - \alpha^2 J_0(\alpha x^*(\alpha))}. \tag{80}$$

Note that, according to (77), the denominator of (80) is less then zero. Therefore, to prove (19), it is required to show that

$$J_0(\alpha x^*(\alpha)) > 0. \tag{81}$$

To show (81), let $h_3(\xi) \triangleq \xi J_1(\xi x^*(\alpha))$. It directly follows from (79) that $h_3(1) - h_3(\alpha) = 0$, and, therefore, there is a $c_3 \in (\alpha,1)$ such that $dh_3(\xi)/d\xi \mid_{\xi=c_3} = c_3 x^*(\alpha)J_0(c_3 x^*(\alpha)) = 0$. It holds from the latter equation that $c_3 x^*(\alpha) = \nu_0$, and, hence, $\alpha x^*(\alpha) < \nu_0$. Inequality (81) is obtained from the latter result. This completes the proof.

APPENDIX C
PROOF OF THEOREM 2

As the two nodes are arbitrarily selected, they are two arbitrary points on $S(O,R_{i,s},R_{o,s})$ (or $D(O,R_{o,d})$). As such, in the case that the nodes are uniformly distributed on $S(O,R_{i,s},R_{o,s})$, we have $P^{(s)} = A_T/(\pi R_{o,s}^2 - \pi R_{i,s}^2)$ where A_T is the area of the R_f-neighborhood of an arbitrary point T on $S(O,R_{i,s},R_{o,s})$. The hashed region in Fig. 10 depicts this neighborhood. Note that, due to the left inequality of (22), the R_f-neighborhood of T is cut by both inner and outer boundaries of $S(O,R_{i,s},R_{o,s})$. Moreover, not only $R_f \ll R_{o,s}$, but also it follows from (22) that $R_f \ll R_{o,s} - (R_{o,s} - R_{i,s}) = R_{i,s}$. The above observations imply that A_T can be well approximated by the area of a rectangle of length $2R_f$ and width $R_{o,s} - R_{i,s}$ (see also Fig. 10). Therefore, we have $P^{(s)} \approx 2R_f/(\pi R_{o,s} + \pi R_{i,s}) \approx R_f/(\pi R_{o,s})$. This proves (23). In the case that the nodes are uniformly distributed on $D(O,R_{o,d})$, we have $P^{(d)} = A_T/(\pi R_{o,d}^2)$ where A_T is the area of the R_f-neighborhood of an arbitrary point T on $D(O,R_{o,d})$. Due to the assumption that $R_f \ll R_{o,d}$, the probability that the distance of T from the disc boundary is less than R_f is negligible, and, hence, $A_T = \pi R_f^2$ with a high probability. This directly establishes (24).

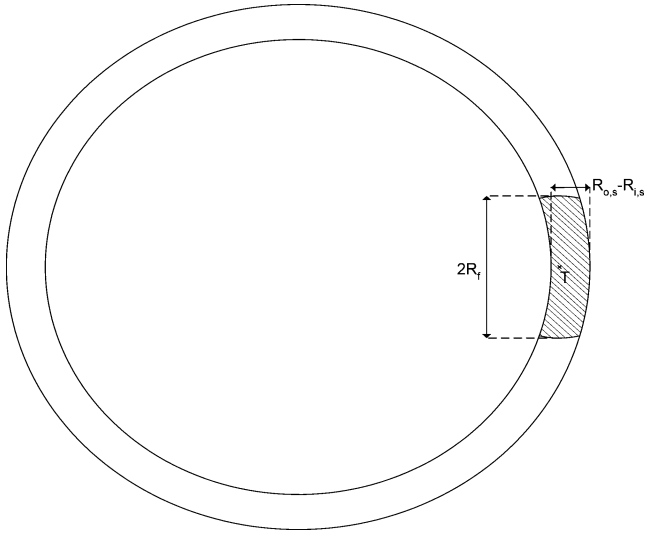

Fig. 10. An R_f-neighborhood of a node on $S(O,R_{i,s},R_o)$.

APPENDIX D
PROOF OF THEOREM 3

Note that

$$\begin{aligned}\tilde{D}_{\text{av}} &= \frac{2\pi}{\int_{-\pi}^{\pi} P_{\text{av}}(\phi)d\phi} \\ &\approx \frac{2\pi}{\int_{-\pi}^{\pi} \frac{1}{K} + \left(1-\frac{1}{K}\right) J_0^2\left(R_{o,s}\beta(\phi)\right) d\phi} \\ &= \frac{K}{1 + \frac{(K-1)}{2\pi}\int_{-\pi}^{\pi} J_0^2\left(\frac{4\pi R_{o,s}\sin\left(\frac{\phi}{2}\right)}{\lambda}\right) d\phi}.\end{aligned} \tag{82}$$

Using the fact that $J_0(x) = \sum_{l=0}^{\infty}((-1)^l/2^{2l}l!l!)x^{2l}$, it can be shown after some manipulation that

$$\begin{aligned}&\int_{-\pi}^{\pi} J_0^2\left(\frac{4\pi R_{o,s}\sin\left(\frac{\phi}{2}\right)}{\lambda}\right) d\phi \\ &\quad = \sum_{l=0}^{\infty} \frac{(-1)^l(2l)!}{2^{2l}l!l!l!l!}\left(\frac{4\pi R_{o,s}}{\lambda}\right)^{2l} \int_{-\pi}^{\pi} \sin^{2l}\left(\frac{\phi}{2}\right) d\phi\end{aligned}$$

$$P_{\mathrm{ns,av}}(\phi)=\frac{\mathbf{1}^T\left(\mathbf{\Sigma}+\frac{\varrho_0^2}{\varsigma}(\mathbf{I}+\mathbf{\Delta})\right)^{-1}\left(\mathrm{E}_{\mathbb{Z}}\left\{\check{\mathbf{M}}_2(\phi,\mathbb{Z})\right\}+\mathrm{E}_{\mathbb{Z}}\left\{\check{\mathbf{M}}_2(\phi,\mathbb{Z})\right\}\right)\left(\mathbf{\Sigma}+\frac{\varrho_0^2}{\varsigma}(\mathbf{I}+\mathbf{\Delta})\right)^{-1}\mathbf{1}}{K\cdot\mathbf{1}^T\left(\mathbf{\Sigma}+\frac{\varrho_0^2}{\varsigma}(\mathbf{I}+\mathbf{\Delta})\right)^{-1}(\mathbf{I}+\mathbf{\Delta})\left(\mathbf{\Sigma}+\frac{\varrho_0^2}{\varsigma}(\mathbf{I}+\mathbf{\Delta})\right)^{-1}\mathbf{1}} \tag{87}$$

$$c_1=\frac{\left(\varrho^2+\frac{\varrho_0^2}{\varsigma}(1+\varrho^2)\right)^{-2}(\mathbf{1}^T\mathbf{1}\mathbf{1}^T\mathbf{1}-\mathbf{1}^T\mathbf{1})}{(K-1)\cdot(1+\varrho^2)\left(\varrho^2+\frac{\varrho_0^2}{\varsigma}(1+\varrho^2)\right)^{-2}\mathbf{1}^T\mathbf{1}}=\frac{1}{1+\varrho^2} \tag{93}$$

$$c_2=\frac{\left(\varrho^2+\frac{\varrho_0^2}{\varsigma}(1+\varrho^2)\right)^{-2}((K-1)\cdot\varrho^2\mathbf{1}^T\mathbf{1}+K\cdot\mathbf{1}^T\mathbf{1}-\mathbf{1}^T\mathbf{1}\mathbf{1}^T\mathbf{1})}{K(K-1)\cdot(1+\varrho^2)\left(\varrho^2+\frac{\varrho_0^2}{\varsigma}(1+\varrho^2)\right)^{-2}\mathbf{1}^T\mathbf{1}}=\frac{\varrho^2}{K\cdot(1+\varrho^2)} \tag{94}$$

$$\begin{aligned}&=\sum_{l=0}^{\infty}\frac{(-1)^l(2l)!}{2^{2l}l!l!l!l!}\left(\frac{4\pi R_{o,s}}{\lambda}\right)^{2l}\cdot 2\pi\frac{\left(\frac{1}{2}\right)_l}{l!}\\&=2\pi\sum_{l=0}^{\infty}\frac{\left(\frac{1}{2}\right)_l\left(\frac{1}{2}\right)_l}{l!l!l!}\cdot\frac{\left(-\left(\frac{4\pi R_{o,s}}{\lambda}\right)^2\right)^l}{l!}\\&=2\pi\,{}_2F_3\left(\frac{1}{2},\frac{1}{2};1,1,1,-\left(\frac{4\pi R_{o,s}}{\lambda}\right)^2\right)\end{aligned} \tag{83}$$

where $(a)_l \triangleq a(a+1)\ldots(a+l-1)$. Inserting (83) into (82), (34) directly follows. To prove (35), let us first denote $\gamma\triangleq 4\pi R_{o,s}/\lambda$ and $x\triangleq\gamma\sin(\phi/2)$. From (82) we have

$$\tilde{D}_{\mathrm{av}}\approx\frac{K}{1+(K-1)\cdot\frac{4}{2\pi}\int_0^{\gamma}\frac{J_0^2(x)}{\gamma\sqrt{1-\left(\frac{x}{\gamma}\right)^2}}dx}. \tag{84}$$

To derive a lower-bound on $\tilde{D}_{\mathrm{av}}$, we obtain an upper-bound on the integral in the denominator of (84). First, note that (28) implies that $J_0(x)\le\sqrt{2/(\pi x)}$ for $x>a$ where a is a positive scalar. Although it can be shown that the latter upper-bound holds in fact for $a=0$, we select a tighter upper-bound on $J_0(x)$ as follows

$$J_0(x)\le g(x)=\begin{cases}1 & x\in\left(0,\frac{2}{\pi}\right)\\ \sqrt{\frac{2}{\pi x}} & x\in\left(\frac{2}{\pi},\infty\right).\end{cases} \tag{85}$$

From (85) we have that

$$\begin{aligned}&\int_0^{\gamma}\frac{J_0^2(x)}{\gamma\sqrt{1-\left(\frac{x}{\gamma}\right)^2}}dx\\&\le\int_0^{2/\pi}\frac{dx}{\gamma\sqrt{1-\left(\frac{x}{\gamma}\right)^2}}+\frac{2}{\pi\gamma}\int_{2/\pi}^{\gamma}\frac{dx}{x\sqrt{1-\left(\frac{x}{\gamma}\right)^2}}\\&=\arcsin\left(\frac{\pi}{2\gamma}\right)+\frac{2}{\pi\gamma}\ln\left(\frac{1+\sqrt{1-\left(\frac{\pi}{2\gamma}\right)^2}}{\frac{\pi}{2\gamma}}\right)\\&\approx\frac{\pi}{2\gamma}+\frac{2}{\pi\gamma}\ln\left(\frac{4\gamma}{\pi}\right).\end{aligned} \tag{86}$$

Using (86) and (84), inequality (35) follows. This completes the proof.

Appendix E
Proof of Theorem 4

First, note that (55) yields (87), shown at the top of the page. From (53) we have

$$\left[\mathrm{E}_{\mathbb{Z}}\left\{\check{\mathbf{M}}_1(\phi,\mathbb{Z})\right\}\right]_{i,k}=\begin{cases}1 & i=k\\ \left|\mathrm{E}\left\{e^{j\beta(\phi)Z}\right\}\right|^2 & i\ne k\end{cases} \tag{88}$$

while from (54) it holds that

$$\left[\mathrm{E}_{\mathbb{Z}}\left\{\check{\mathbf{M}}_2(\phi,\mathbb{Z})\right\}\right]_{i,k}=[\mathbf{\Sigma}]_{i,k}\left[\mathrm{E}_{\mathbb{Z}}\left\{\check{\mathbf{M}}_1(\phi,\mathbb{Z})\right\}\right]_{i,k}. \tag{89}$$

Note that $e^{j\beta(\phi)Z}$ in (88) is given by (12) when the DBF nodes are selected from a single ring and by (44) when they are selected from multiple concentric rings. In either case, it follows from (13) and (43) that

$$\left[\mathrm{E}_{\mathbb{Z}}\left\{\check{\mathbf{M}}_1(\phi,\mathbb{Z})\right\}\right]_{i,k}=\begin{cases}1 & i=k\\ \frac{KP_{\mathrm{av}}(\phi)-1}{K-1} & i\ne k.\end{cases} \tag{90}$$

Using (89) and (90), we obtain

$$\begin{aligned}\mathrm{E}_{\mathbb{Z}}\left\{\check{\mathbf{M}}_1(\phi,\mathbb{Z})\right\}&=\frac{KP_{\mathrm{av}}(\phi)-1}{K-1}\cdot\mathbf{1}\mathbf{1}^T\\&\quad+\left(1-\frac{KP_{\mathrm{av}}(\phi)-1}{K-1}\right)\cdot\mathbf{I}\end{aligned} \tag{91}$$

$$\begin{aligned}\mathrm{E}_{\mathbb{Z}}\left\{\check{\mathbf{M}}_2(\phi,\mathbb{Z})\right\}&=\frac{KP_{\mathrm{av}}(\phi)-1}{K-1}\cdot\mathbf{\Sigma}\\&\quad+\left(1-\frac{KP_{\mathrm{av}}(\phi)-1}{K-1}\right)\cdot\mathbf{\Delta}.\end{aligned} \tag{92}$$

Using (91) and (92) in (87) and following a straightforward manipulation, (56)–(58) are obtained. To prove (59), note that when $\mathbf{\Sigma}=\varrho^2\mathbf{I}$ we have (93) and (94), shown at the top of the page. Substituting (93) and (94) in (56), (59) follows. This completes the proof.

REFERENCES

[1] H. Ochiai, P. Mitran, H. V. Poor, and V. Tarokh, "Collaborative beamforming for distributed wireless ad hoc sensor networks," *IEEE Trans. Signal Process.*, vol. 53, no. 11, pp. 4110–4124, Nov. 2005.

[2] M. F. A. Ahmed and S. A. Vorobyov, "Collaborative beamforming for wireless sensor networks with Gaussian distributed sensor nodes," *IEEE Trans. Wireless Commun.*, vol. 8, no. 2, pp. 638–643, Feb. 2009.

[3] L. Dong, A. P. Petropulu, and H. V. Poor, "A cross-layer approach to collaborative beamforming for wireless ad hoc networks," *IEEE Trans. Signal Process.*, vol. 56, no. 7, pp. 2981–2993, Jul. 2008.

[4] R. Mudumbai, G. Barriac, and U. Madhow, "On the feasibilty of distributed beamforming in wireless sensor networks," *IEEE Trans. Wirless Commun.*, vol. 6, no. 4, pp. 1754–1763, Apr. 2007.

[5] A. G. Marques, X. Wang, and G. B. Giannakis, "Minimizing transmit power for coherent communications in wireless sensor networks with finite-rate feedback," *IEEE Trans. Signal Process.*, vol. 56, no. 9, pp. 4446–4457, Sep. 2008.

[6] V. Havary-Nassab, S. Shahbazpanahi, A. Grami, and Z.-Q. Luo, "Distributed beamforming for relay networks based on second-order statistics of the channel state information," *IEEE Trans. Signal Process.*, vol. 56, no. 9, pp. 4306–4316, Sep. 2008.

[7] Y. Jing and H. Jafarkhani, "Network beamforming using relays with perfect channel information," *IEEE Trans. Inf. Theory*, vol. 55, no. 6, pp. 2499–2517, Jun. 2009.

[8] A. El-Keyi and B. Champagne, "Collaborative uplink transmit beamforming with robustness against channel estimation errors," *IEEE Trans. Veh. Technol.*, vol. 58, no. 1, pp. 126–139, Jan. 2009.

[9] R. Mudumbai, D. R. Brown, U. Madhow, and H. V. Poor, "Distributed transmit beamforming: Challenges and recent progress," *IEEE Commun. Mag.*, vol. 47, no. 2, pp. 102–110, Feb. 2009.

[10] S. Boyd, A. Ghosh, B. Prabhakar, and D. Shah, "Randomized gossip algorithms," *IEEE Trans. Inf. Theory*, vol. 52, no. 6, pp. 2508–2530, Jun. 2006.

[11] T. C. Aysal, M. J. Coates, and M. G. Rabbat, "Distributed average consensus with dithered quantization," *IEEE Trans. Signal Process.*, vol. 56, no. 10, pp. 4905–4918, Oct. 2008.

[12] R. Karp, C. Schindelhauser, S. Shenker, and B. Vöking, "Randomized rumor spreading," in *Proc. Symp. Foundations of Computer Science*, 2000, pp. 564–574.

[13] D. R. Brown, III and H. V. Poor, "Time-slotted round-trip carrier synchronization for distributed beamforming," *IEEE Trans. Signal Process.*, vol. 56, no. 11, pp. 5630–5643, Nov. 2008.

[14] P. Gupta and P. R. Kumar, "Critical power for asymptotic connectivity in wireless networks," in *Stochastic Analysis, Control, Optimization and Applications: A Volume in Honor of W. H. Fleming*, W. M. McEneany, G. Yin, and Q. Zhang, Eds. Boston, MA: Birkhauser, 1998, pp. 547–566.

[15] C. Bettstetter, "On the connectivity of ad hoc networks," *Computer J.*, vol. 47, pp. 432–447, Jul. 2004.

[16] M. Haenggi, "On distances in uniformly random networks," *IEEE Trans. Inf. Theory*, vol. 51, no. 10, pp. 3584–3586, Oct. 2005.

[17] S. Mukherjee, D. Avidor, and K. Hartman, "Connectivity, power, and energy in a multihop cellular-packet system," *IEEE Trans. Veh. Technol.*, vol. 56, no. 2, pp. 818–836, Mar. 2007.

[18] W. Ye, J. Heidemann, and D. Estrin, "Medium access control with coordinated adaptive sleeping for wireless sensor networks," *IEEE/ACM Trans. Netw.*, vol. 12, no. 3, pp. 493–506, Jun. 2004.

[19] M. Desai and D. Manjunath, "On the connectivity in finite ad hoc networks," *IEEE Commun. Lett.*, vol. 6, no. 10, pp. 437–439, Oct. 2002.

[20] C. Bettstetter and C. Hartmann, "Connectivity of wireless multihop networks in a shadow fading environment," *ACM/Springer Wireless Netw.*, vol. 11, pp. 571–579, Sep. 2005.

[21] O. Younis and S. Fahmy, "HEED: A hybrid, energy-efficient, distributed clustering approach for ad hoc sensor networks," *IEEE Trans. Mob. Comput.*, vol. 3, no. 4, pp. 366–379, Oct.–Dec. 2004.

[22] F. D. Tolba, D. Magoni, and P. Lorenz, "Connectivity, energy and mobility driven clustering algorithm for mobile ad hoc networks," in *Proc. GLOBECOM'07*, pp. 2786–2790.

Keyvan Zarifi (S'04–M'08) received the Ph.D. degree (with the highest honors) in electrical and computer engineering from Darmstadt University of Technology, Darmstadt, Germany, in 2007.

From January 2002 until March 2005, he was with the Department of Communication Systems, University of Duisburg-Essen, Duisburg, Germany. From April 2005 until September 2007, he was with the Darmstadt University of Technology. From September 2002 until March 2003, he was a Visiting Scholar at the Department of Electrical and Computer Engineering, McMaster University, Hamilton, ON, Canada. Since September 2007, he has been jointly with Institut National de la Recherche Scientifique-Énergie, Matériaux, et Télécommunications (INRS-EMT), Université du Québec, and Concordia University, Montreal, QC, Canada, as a Postdoctoral Fellow. His research interests include statistical signal processing, wireless sensor networks, MIMO and cooperative communications, and blind estimation and detection techniques.

In 2008, Mr. Zarifi has received Postdoctoral Fellowship from the Natural Sciences and Engineering Research Council of Canada (NSERC).

Ali Ghrayeb (S'97–M'00–SM'06) received the Ph.D. degree in electrical engineering from the University of Arizona, Tucson, in 2000.

He is currently an Associate Professor with the Department of Electrical and Computer Engineering, Concordia University, Montreal, QC, Canada. He holds a Concordia University Research Chair in Wireless Communications. He is the coauthor of the book *Coding for MIMO Communication Systems* (Wiley, 2008). His research interests include wireless and mobile communications, error correcting coding, MIMO systems, wireless cooperative networks, and CDMA/WCDMA systems.

Dr. Ghrayeb has instructed/co-instructed technical tutorials at several major IEEE conferences. He serves as an Associate Editor of the IEEE TRANSACTIONS ON VEHICULAR TECHNOLOGY and IEEE TRANSACTIONS ON SIGNAL PROCESSING. He served as an Associate Editor of the Wiley *Wireless Communications and Mobile Computing Journal* from 2004–2008.

Sofiène Affes (S'94–M'95–SM'04) received the Diplôme d'Ingénieur in telecommunications in 1992, and the Ph.D. degree with honors in signal processing in 1995, both from the École Nationale Supérieure des Télécommunications (ENST), Paris, France.

He has been since with INRS-EMT, University of Quebec, Montreal, Canada, as a Research Associate from 1995 until 1997, as an Assistant Professor till 2000, then as an Associate Professor till 2009. Currently he is a Full Professor in the Wireless Communications Group. His research interests are in wireless communications, statistical signal and array processing, adaptive space-time processing and MIMO. From 1998 to 2002, he has been leading the radio design and signal processing activities of the Bell/Nortel/NSERC Industrial Research Chair in Personal Communications at INRS-EMT. Since 2004, he has been actively involved in major projects in wireless of Partnerships for Research on Microelectronics, Photonics and Telecommunications (PROMPT).

Professor Affes was the co-recipient of the 2002 Prize for Research Excellence of INRS. He currently holds a Canada Research Chair in Wireless Communications and a Discovery Accelerator Supplement Award from Natural Sciences and Engineering Research Council of Canada (NSERC). In 2006, he served as a General Co-Chair of the IEEE VTC'2006-Fall Conference, Montreal. In 2008, he received from the IEEE Vehicular Technology Society the IEEE VTC Chair Recognition Award for exemplary contributions to the success of IEEE VTC. He currently acts as a member of the Editorial Board of the IEEE TRANSACTIONS ON WIRELESS COMMUNICATIONS and of the Wiley *Journal on Wireless Communications & Mobile Computing*.